Publications of the Astronomical Society of Australia (PASA), Vol. 31, e024, 23 pages (2014).

doi:10.1017/pasa.2014.17

The Catalogue of Stellar Parameters from the Detached Double-Lined Eclipsing Binaries in the Milky Way

Z. Eker[1,6], S. Bilir[2], F. Soydugan[3,4], E. Yaz Gökçe[2], E. Soydugan[3,4], M. Tüysüz[3,4], T. Şenyüz[3,4] and O. Demircan[4,5]

[1]Department of Space Sciences and Technologies, Faculty of Sciences, Akdeniz University, Antalya 07058, Turkey
[2]Department of Astronomy and Space Sciences, Faculty of Sciences, Istanbul University, 34119, Turkey
[3]Department of Physics, Faculty of Sciences and Arts, Çanakkale Onsekiz Mart University, 17100 Çanakkale, Turkey
[4]Astrophysics Research Center and Ulupınar Observatory, Çanakkale Onsekiz Mart University, 17100 Çanakkale, Turkey
[5]Department of Space Science and Technologies, Faculty of Sciences and Arts, Çanakkale Onsekiz Mart University, 17020 Çanakkale, Turkey
[6]Email: eker@akdeniz.edu.tr

(Received August 19, 2013; Accepted February 28, 2014)

Abstract

The most accurate stellar astrophysical parameters were collected from the solutions of the light and the radial velocity curves of 257 detached double-lined eclipsing binaries in the Milky Way. The catalogue contains masses, radii, surface gravities, effective temperatures, luminosities, projected rotational velocities of the component stars, and the orbital parameters. The number of stars with accurate parameters increased 67% in comparison to the most recent similar collection by Torres, Andersen, & Giménez (2010). Distributions of some basic parameters were investigated. The ranges of effective temperatures, masses, and radii are $2\,750 < T_{\rm eff}({\rm K}) < 43\,000$, $0.18 < M/M_{\odot} < 33$, and $0.2 < R/R_{\odot} < 21.2$, respectively. Being mostly located in one kpc in the Solar neighborhood, the present sample covers distances up to 4.6 kpc within the two local Galactic arms, Carina-Sagittarius and Orion Spur. The number of stars with both mass and radius measurements better than 1% uncertainty is 93, better than 3% uncertainty is 311, and better than 5% uncertainty is 388. It is estimated from the Roche lobe filling factors that 455 stars (88.5% of the sample) are spherical within 1% of uncertainty.

Keywords: astronomical data based: catalogues – stars: binaries: eclipsing – stars: fundamental parameters – stars: binaries: spectroscopic

1 INTRODUCTION

Nearly 60% or more of the Solar neighborhood stars are binaries or multiple systems (Duquennoy & Mayor 1993). Binaries are important for astrophysicists not only because they over populate single stars, but also because they provide basic stellar parameters as independent observed quantities used in testing astrophysical theories. Stellar masses can be determined directly via application of Kepler's law for the visual binaries if apparent orbital parameters were calibrated to be real. A calibration is possible for a visual pair if its distance (parallax) is known. Reliable stellar masses could also be obtained from the radial velocity curves without distance, but only if orbital inclinations were known. The resolved double stars (visual binaries confirmed to be spectroscopic binaries), therefore, are a special case to provide reliable stellar masses, since the orbital inclinations are from the apparent orbit and the absolute orbital sizes are from the radial velocity curves.

Gainfully, the light curves of eclipsing binaries could provide orbital inclinations and the radii relative to the semi-major axis of the orbit. But, if both stars are resolved spectroscopically, accurately determined radii and masses could be obtained from the simultaneous solutions of the light and the radial velocity curves. In addition to the radii, which are not available from visual binaries, the eclipsing spectroscopic binaries provide masses, effective temperatures, and the absolute dimensions of the orbit, from which absolute brightness could be calculated. Provided with a parallax, either the physical parameters or the parallax could mutually be tested by comparing the photometric and the trigonometric distance moduli. Otherwise, a proper solution would provide not only the most reliable stellar parameters, but also a reliable photometric distance (parallax) as an independent quantity.

The critical compilations of stellar parameters and absolute dimensions of binary components were initiated, and continued with increasing quantity and quality, especially by

Popper (1980) and Harmanec (1988). Andersen (1991) collected accurate stellar masses and radii with uncertainties less than 2% from the detached, double-lined eclipsing systems. The list contained 45 (90 stars) binaries which are all non-interacting, so that each star could be accepted as if evolved as single stars. Accuracies of 1%–2% were found to be significant for deeper astrophysical insight than merely improving the spectrum of masses and radii. Due to great sensitivity of other parameters, only limited amount of useful results could be extracted up to ±5% uncertainties.

Malkov (1993) announced a catalogue of astrophysical parameters of binary systems containing 114 systems including all pre- and out-of-main-sequence, contact, and semi-contact systems. Gorda & Svechnikov (1998) collected stellar masses and radii with accuracies better than 2%–3% from photometric, geometric, and absolute elements of 112 eclipsing binaries with both components on the main sequence, for studying the mass-luminosity and mass-radius relations. Ages and metallicities for the components of 43 eclipsing binaries with lines of both components visible on the spectra were studied by Kovaleva (2001).

As the number of stars with reliable physical parameters is increasing, the studies concentrated more on the precision and accuracy. Therefore, Ibanoğlu et al. (2006) did not combine 74 double-lined detached eclipsing Algols and 61 semi-detached Algols when plotting mass-radius, mass-$T_{\rm eff}$, radius-$T_{\rm eff}$, and mass-luminosity data. Lastennet & Valls-Gabaud (2002) compiled 60 non-interacting, well-detached systems with typical errors smaller than 2% for masses and radii, while 5% for the effective temperatures. The core of the sample was the large catalogue of Andersen (1991). As being satisfied with 10% accuracy for the main-sequence stars, Hillenbrand & White (2004) studied dynamical mass constraints on pre-main-sequence evolutionary tracks with 148 stars, 88 are on the main-sequence, 27 are on the pre-main-sequence, and 33 are on the post-main-sequence, where the source of data were Andersen (1991), Ribas et al. (2000), and Delfosse et al. (2000). Despite, the number of eclipsing binaries was 6 330 in 'the catalogue of eclipsing binaries' by Malkov et al. (2006), but Malkov (2007) was able to select only 215 stars (114 binaries) which are detached-main-sequence and double-lined eclipsing binary with uncertainties for masses, radii, $\log T_{\rm eff}$, $\log L$, and $\log M$ were assumed to be 10, 10%, 0.03, 0.03, and 0.1 mag or better respectively.

Eclipsing binaries are not only recognised with their accuracy, but also known to have larger spectrum of mass range, especially towards larger masses in compared to visual binaries including *Hipparcos* detections (Malkov 2003). Improvements in observing and analysis techniques never stop, and collection of reliable light and radial velocity curve solutions continues. Recently, Torres et al. (2010) updated the critical compilation of detached, double-lined eclipsing binaries with accurate masses and radii. Superseding Andersen (1991) list, this new list contains 190 stars (94 eclipsing binaries and α Cen). In order to fill the gaps in different mass ranges, further compilations on the accurate absolute dimensions of the eclipsing double-lined spectroscopic binaries are inevitable.

The aim of this paper is to present our compilation of 514 stars which are from 257 detached eclipsing double-lined spectroscopic binaries (SB2) of the Milky Way. The number of stars in our list with reliable masses, spectroscopic mass ratios, orbital inclinations, radii, $T_{\rm eff}$, $\log g$, and $v \sin i$ values as collected from the literature supersede similar compilations before. Selecting criteria and data collection from binaries and the descriptions of the quality of the data are given in Section 2. The H-R diagram, space distributions, and how good a typical single star represented are discussed in Section 3, and finally, conclusions are provided in Section 4.

2 THE CATALOGUE

2.1 Selecting criteria and data collection

The basic stellar (masses, radii, $T_{\rm eff}$, $\log g$, $v \sin i$) and orbital (radial velocity amplitudes K_1, K_2, mass ratio q, orbital period $P_{\rm orb}$, orbital inclination i, semi-major axis a, eccentricity e) parameters have been collected from the published material through literature from the simultaneous solutions of light and radial velocity curves of 257 detached eclipsing and double-lined spectroscopic binaries in our Galaxy. The collections were complete by the date 2013 January 2. The strict initial criterion was first to make an eye inspection to the light and the radial velocity curves, to make sure the system is detached, and have sufficient number of observed data on both curves to assure acceptable accuracy. The systems having W UMa- and β Lyr-type light curves, which are known as contact and semi-contact systems respectively, were avoided. The near contact systems showing noticeable proximity effects such as ellipticity and reflection on their light curves were also avoided. Another criterion was to make sure all systems are in the Milky Way, so as to avoid complexities involving extragalactic origins and to form a homogeneous sample.

If there were such systems studied more than once, that is, the light and the radial velocity curves determined and solved in various studies, the most recent solutions which include or compare to the previous solutions were preferred. We were aware of the fact that some of the chromosphericaly active binaries are possible to fulfil the above criteria. For example, if a detached, double-lined eclipsing binary is one of the studied chromospheric aly active binaries with starspots, we were keen to accept stellar parameters only if spotless clean solutions exist, in order to avoid negative contribution of starspots on the stellar parameters. Therefore, 24 binaries in the current collected sample are also contained in third edition of the catalogue of Chromosphericaly Active Binaries (CABs) by Eker et al. (2008).

2.2 Impact of selecting criteria and observational bias

Binaries have numerous advantages over single stars when determining basic stellar parameters, like masses, radii,

effective temperatures, etc., through observations. Direct measurements of stellar radii come only from the light curve analysis of eclipsing binaries. Therefore, the first selection criterion is to require eclipses.

After many years of observational experience today for recognising eclipsing nature of a light curve, it's always useful for one to remember the famous debate, binary versus pulsation (Shapley 1914; Eddington 1918; Hall 1994), in the beginning of the 20th century. Even if one is sure, the light curve is in eclipsing nature, the light curve alone is not sufficient to extract absolute sizes of the orbit and radii of the component stars unless apparent angular size and distance of the eclipsing system are known independently. Radial velocity curves of eclipsing SB2 binaries not only could confirm consistency of eclipses but also provide the absolute size of the orbit by using the value of orbital inclination from the light curve analysis. Consequently, absolute sizes of radii could be computed from the eclipse durations and absolute size of the orbit. Therefore, for the second selection criterion, each eclipsing binary must be an SB2 system.

Eclipsing light curves and radial velocity curves of SB2, however, do not always assure basic stellar parameters (mass, radius, effective temperature, surface gravity, luminosity, etc.) as accurate as usable by the theoretical astronomers to compare and test their astrophysical theories. Therefore, complex cases associated with these two basic criteria must be removed by additional selection rules. So, the third selection criterion is established as 'avoiding extragalactic systems' in order to form a homogeneous sample representing binaries in the Milky Way and in the Solar neighborhood.

Most stellar astrophysical theories start with the simplest assumptions, e.g. being single, spherical, non-rotating, not-pulsating, etc. Complexities, such as mass loss, convective overshoot, rotation, pulsation, etc. were added later. Today there are many theoretical stellar evolution models (i.e. Pols et al. 1998; Demarque et al. 2004; Girardi et al. 2010; Ekstrom et al. 2012) competing. Apparently those models, which involve single stars, were tested and/or improved by comparing observational parameters mostly comes from binaries advantageous to provide most accurate data. Moreover, single star evolution becomes invalid if it is an interactive binary and experience mass transfer. Therefore, similar kinds of data from single stars are not only poor thus not useful but also not free from many severe complexities. For example, one can never be sure a single star is really single and evolved as a single. de Mink, Langer, & Izzard (2011) claimed 'the only unambiguous identification of true single stars is possible in detached binaries, which contain two main-sequence stars'. Therefore, for the fourth selection criterion in this study, 'avoid interacting binaries known to be involving mass transfer, such as W UMa and β Lyr types'.

Near contact binaries, with strong proximity effects, still introduce complexities involving strong tidal synchronisation, deformation of shapes, and mutual irradiations of the component stars. So, fifth selection criterion, 'avoid systems with proximity effects', must be added.

Active solar-type stars with starspots may introduce minor but unavoidable complexity causing determined radii, relative temperatures to be less accurate. Therefore, sixth selection criterion, 'avoid stellar activity, accept the spotless solutions'.

2.3 Description and quality of the data

The catalogue is available in an electronic format (Table S1, available online). The content of the catalogue is organised as a table of 257 rows and 60 columns. Thus, each row of data belongs to a detached eclipsing binary, which is an SB2 system. The columns and their descriptions were given in Table 1, where one may notice the data were carefully referenced for interested readers who want to see original sources. Original sources, however, are heterogeneous to use the older and the newer values of $GM_{\odot}$ and $R_{\odot}$ when deriving the observed masses and radii. Since contributing uncertainty of those constants is not entirely negligible (0.23%) as estimated by Torres et al. (2010), by means of their formulae, the collected masses and radii were homogenised using $GM_{\odot} = 1.3271244 \times 10^{20}$ m^3 s^{-2} (Standish 1995) and $R_{\odot} = 6.9566 \times 10^8$m (Haberreiter, Schmutz, & Kosovichev 2008). Next, surface gravities and luminosities recomputed from the homogenised quantities. Those re-evaluated quantities and their associated errors are listed in Table 2 where columns are self explanatory.

Containing 514 stars (257 binaries), the present catalogue supersedes the most recent collection by Torres et al. (2010) with 190 stars (94 eclipsing systems and α Cen). Both catalogues are similar in a sense, containing detached eclipsing binaries with an exception that α Cen being astrometric binary is excluded. Moreover, extragalactic binary OGLE 051019, which is in the list of Torres et al. (2010), is also excluded because it is not in our Galaxy. As a result, only 93 binaries are common in both catalogues, hence there is substantial amount of excess ($257 - 93 = 164$) in the present catalogue. However, it is prudent to compare the quality of the data rather than a plain number. Torres et al. (2010) preferred to collect binaries with the masses and radii of both stars to be known within errors of $\pm 3\%$ accuracy or better. Rather than binaries, present study concentrates on component stars and collects individual stars with most accurate masses and radii. In the present sample, the number of stars with both mass and radius within $\pm 3\%$ accuracy or better is 311. The number implies 67% more stars than Torres et al. (2010) with similar accuracy. Among the 311, 292 stars are matched binaries, thus the number of Galactic binaries with similar accuracy increased from 93 to 146 (57%) in this study. When comparing the most accurate data, that is, the number of individual stars with both mass and radius with accuracies $\pm 1\%$ or better are 93 and 43 in the present list and in the list of Torres et al. (2010), respectively. Such improvements justify the publication of the present catalogue.

Among the 93 binaries which are common between the present catalogue and the catalogue of Torres et al. (2010),

Table 1. Column descriptions of the catalogue data.

Column	Description	Remark
1	ID	Order number
2	Star name	The most common name
3	HD	Henry Draper catalogue number
4	Hip	*Hipparcos* catalogue number
5	SAO	Smithsonian Astrophysical Observatory star catalogue number
6	α (hh:mm:ss.ss)	Right ascension in J2000
7	δ (dd:mm:ss.ss)	Declination in J2000
8	l (°)	Galactic longitude
9	b (°)	Galactic latitude
10	Spt Type	Spectral types of components
11	Ref	Reference to spectral types
12	V (mag)	Johnson V apparent magnitude of system
13	π (mas)	Trigonometric parallax
14	σ_π (mas)	Standard error of π
15	Ref	Reference to π and σ_π
16	γ (kms^{-1})	Centre of mass velocity of orbit
17	σ_γ (kms^{-1})	Standard error of γ
18	Ref	Reference to γ
19	K_1 (kms^{-1})	Radial velocity amplitude of primary
20	σ_{K_1} (kms^{-1})	Standard error of K_1
21	K_2 (kms^{-1})	Radial velocity amplitude of secondary
22	σ_{K_2} (kms^{-1})	Standard error of K_2
23	q	Mass ratio of components
24	Ref	Reference to q
25	$P_{\rm orb}$ (day)	Orbital period
26	Ref	Reference to P
27	a ($R_\odot$)	Semi-major axis of orbit
28	σ_a ($R_\odot$)	Standard error of a
29	i (°)	Orbital inclination
30	e	Orbital eccentricity
31	Ref	Reference to a, e, i
32	FF1 (%)	Roche lobe filling ratio of primary
33	FF2 (%)	Roche lobe filling ratio of secondary
34	M_1 ($M_\odot$)	Mass of primary
35	σ_{M_1} ($M_\odot$)	Standard error of M_1
36	M_2 ($M_\odot$)	Mass of secondary
37	σ_{M_2} ($M_\odot$)	Standard error of M_2
38	R_1 ($R_\odot$)	Radius of primary
39	σ_{R_1} ($R_\odot$)	Standard error of R_1
40	R_2 ($R_\odot$)	Radius of secondary
41	σ_{R_2} ($R_\odot$)	Standard error of R_2
42	Ref	References to M_1, M_2, R_1 and R_2
43	T_1 (K)	Effective temperature of primary
44	σ_{T_1} (K)	Standard error of T_1
45	T_2 (K)	Effective temperature of secondary
46	σ_{T_2} (K)	Standard error of T_2
47	Ref	References to T_1 and T_2
48	$\log g_1$ (cms^{-2})	Surface gravity on primary
49	$\sigma_{\log g_1}$ (cms^{-2})	Standard error of $\log g_1$
50	$\log g_2$ (cms^{-2})	Surface gravity on secondary
51	$\sigma_{\log g_2}$ (cms^{-2})	Standard error of $\log g_2$
52	Ref	References to $\log g_1$ and $\log g_2$
53	$v_1 \sin i$ (kms^{-1})	Projected equatorial rotational velocity of primary
54	$\sigma_{v_1 \sin i}$ (kms^{-1})	Standard error of $v_1 \sin i$
55	$v_2 \sin i$ (kms^{-1})	Projected equatorial rotational velocity of secondary
56	$\sigma_{v_2 \sin i}$ (kms^{-1})	Standard error of $v_2 \sin i$
57	Ref	Reference to $v_1 \sin i$ and $v_2 \sin i$
58	d (pc)	Distance of binary
59	σ_d (pc)	Standard error of distance
60	Ref	Reference to the distance

PASA, 31, e024 (2014)
doi:10.1017/pasa.2014.17

Table 2. Homogenized parameters and orbital sizes of detached, double-lined eclipsing binaries.

ID	System	M_1 ($M/M_\odot$)	M_2 ($M/M_\odot$)	R_1 ($R/R_\odot$)	R_2 ($R/R_\odot$)	T_1 (K)	T_2 (K)	$\log L_1$ ($L/L_\odot$)	$\log L_2$ ($L/L_\odot$)	$\log g_1$ (cgs)	$\log g_2$ (cgs)	a ($R_\odot$)
1	DV Psc	0.677±0.019	0.475±0.010	0.685±0.030	0.514±0.020	4450±8	3614±8	-0.782±0.040	-1.393±0.035	4.597±0.042	4.693±0.037	2.015±0.101
2	MU Cas	4.657±0.100	4.575±0.090	4.192±0.050	3.671±0.040	14750±500	15100±500	2.873±0.064	2.799±0.063	3.861±0.014	3.969±0.013	40.026±0.190
3	V69-47 Tuc	0.876±0.005	0.859±0.006	1.316±0.005	1.163±0.006	5945±150	5959±150	0.288±0.046	0.185±0.046	4.142±0.004	4.241±0.005	48.324±0.010
4	YZ Cas	2.308±0.010	1.347±0.010	2.547±0.030	1.359±0.020	9200±300	6700±250	1.620±0.062	0.524±0.072	3.989±0.011	4.301±0.013	17.584±0.070
5	NGC188 KR V12	1.102±0.007	1.080±0.007	1.425±0.019	1.374±0.019	5900±100	5875±100	0.344±0.033	0.305±0.033	4.173±0.012	4.196±0.013	19.021±0.040
6	V364 Cas	1.684±0.094	1.559±0.095	1.600±0.010	1.600±0.010	7816±86	7780±86	0.933±0.020	0.925±0.020	4.256±0.026	4.223±0.028	8.318±0.010
7	CD-80 28	1.380±0.055	1.385±0.055	3.209±0.335	4.123±0.416	—	—	—	—	3.565±0.104	3.349±0.100	23.764±0.508
8	zet Phe	3.922±0.045	2.545±0.026	2.853±0.020	1.854±0.020	14550±350	11910±200	2.515±0.044	1.793±0.032	4.121±0.008	4.308±0.010	11.036±0.040
9	AI Phe	1.197±0.005	1.238±0.004	2.935±0.048	1.819±0.024	6310±150	5010±120	1.089±0.046	0.272±0.045	3.581±0.015	4.011±0.012	47.881±0.050
10	CO And	1.289±0.007	1.264±0.007	1.727±0.021	1.694±0.017	6140±130	6170±130	0.580±0.040	0.572±0.039	4.074±0.011	4.082±0.009	13.650±0.030
11	V459 Cas	2.015±0.030	1.962±0.030	2.010±0.013	1.966±0.013	9140±300	9100±300	1.403±0.061	1.377±0.062	4.136±0.009	4.144±0.009	27.680±0.110
12	2MASSJ01132817-3821024	0.613±0.030	0.445±0.019	0.596±0.020	0.445±0.024	3750±250	3085±300	-1.200±0.140	-1.793±0.225	4.675±0.038	4.790±0.054	2.502±0.040
13	UV Psc	0.983±0.009	0.764±0.005	1.117±0.020	0.835±0.030	5780±100	4750±80	0.097±0.035	-0.497±0.045	4.335±0.016	4.478±0.033	4.588±0.010
14	BD-08 308	0.489±0.009	0.443±0.009	1.126±0.380	1.019±0.373	—	—	—	—	4.024±0.488	4.068±0.572	13.481±0.115
15	2MASS J01542930+0053266	0.515±0.023	0.548±0.025	0.601±0.078	0.574±0.087	3800	3600	-1.170	-1.304	4.592±0.133	4.659±0.159	8.201±0.113
16	NSVS 06507557	0.656±0.086	0.279±0.045	0.603±0.030	0.445±0.024	3960±80	3365±80	-1.095±0.060	-1.642±0.067	4.694±0.078	4.587±0.094	2.645±0.121
17	V615 Per	4.075±0.055	3.178±0.051	2.292±0.141	1.904±0.094	15000±500	11000±500	2.378±0.087	1.678±0.101	4.328±0.057	4.381±0.046	46.674±0.280
18	V618 Per	2.332±0.031	1.558±0.025	1.636±0.069	1.318±0.069	11000±1000	8000±1000	1.546±0.203	0.805±0.311	4.378±0.039	4.391±0.049	22.736±0.130
19	V505 Per	1.272±0.001	1.254±0.001	1.288±0.014	1.267±0.014	6512±21	6462±12	0.428±0.011	0.400±0.010	4.323±0.010	4.331±0.010	14.972±0.010
20	AG Ari	2.164±0.070	2.148±0.070	2.232±0.023	2.074±0.022	10300±250	9800±230	1.702±0.045	1.552±0.044	4.076±0.017	4.137±0.017	10.740±0.080
21	BD+11 359	1.356±0.008	1.137±0.007	1.822±0.360	1.282±0.290	—	—	—	—	4.049±0.218	4.278±0.262	13.417±0.040
22	XY Cet	1.773±0.016	1.615±0.014	1.876±0.035	1.776±0.029	7870±115	7620±125	1.084±0.031	0.98±0.0330	4.140±0.017	4.147±0.015	12.499±0.040
23	CW Eri	1.583±0.020	1.327±0.010	2.093±0.050	1.569±0.070	6840±86	6561±100	0.935±0.031	0.612±0.050	3.996±0.022	4.170±0.041	11.731±0.050
24	V799 Cas	3.081±0.400	2.970±0.400	3.231±0.140	3.201±0.140	11550±14	11210±14	2.222±0.039	2.162±0.040	3.908±0.074	3.900±0.076	29.912±1.601
25	AE For	0.637±0.004	0.625±0.003	0.673±0.030	0.633±0.030	4100	4055±6	-0.940	-1.012±0.043	4.586±0.041	4.631±0.043	4.297±0.010
26	V570 Per	1.425±0.006	1.328±0.006	1.494±0.110	1.354±0.110	6842±25	6580±70	0.643±0.070	0.489±0.080	4.243±0.069	4.298±0.077	9.051±0.010
27	TV Cet	1.385±0.052	1.265±0.051	1.484±0.020	1.221±0.010	6902±150	6575±150	0.652±0.041	0.398±0.042	4.237±0.021	4.367±0.019	25.388±0.252
28	TZ For	1.945±0.030	2.045±0.060	3.974±0.090	8.349±0.120	6350±100	5000±100	1.363±0.035	1.592±0.039	3.529±0.021	2.906±0.018	119.419±0.080
29	SDSS-MEB-1	0.272±0.020	0.240±0.022	0.268±0.009	0.248±0.008	3320±130	3300±130	-2.106±0.081	-2.184±0.081	5.016±0.046	5.029±0.052	1.850±0.050

PASA, 31, e024 (2014)
doi:10.1017/pasa.2014.17

Table 2. Continued.

ID	System	M_1 ($M/M_\odot$)	M_2 ($M/M_\odot$)	R_1 ($R/R_\odot$)	R_2 ($R/R_\odot$)	T_1 (K)	T_2 (K)	$\log L_1$ ($L/L_\odot$)	$\log L_2$ ($L/L_\odot$)	$\log g_1$ (cgs)	$\log g_2$ (cgs)	a ($R_\odot$)
30	2MASSJ03262072+0312362	0.527±0.002	0.491±0.001	0.505±0.008	0.471±0.009	3330±60	3270±60	-1.550±0.036	-1.643±0.038	4.753±0.014	4.783±0.017	5.758±0.010
31	GJ 3236	0.375±0.016	0.280±0.015	0.383±0.006	0.283±0.004	3310±110	3241±108	-1.801±0.064	-2.101±0.064	4.846±0.024	4.982±0.027	3.074±0.040
32	EY Cep	1.524±0.008	1.500±0.014	1.463±0.010	1.468±0.010	7090±150	6970±150	0.686±0.039	0.6600±0.040	4.291±0.006	4.281±0.007	24.285±0.060
33	V1229 Tau	2.221±0.027	1.565±0.015	1.844±0.037	1.587±0.042	10025±620	7262±380	1.489±0.125	0.799±0.106	4.253±0.019	4.231±0.024	11.957±0.020
34	V1130 Tau	1.306±0.008	1.392±0.008	1.490±0.010	1.784±0.011	6650±70	6625±70	0.591±0.020	0.741±0.020	4.208±0.006	4.079±0.006	5.045±0.010
35	IQ Per	3.513±0.040	1.733±0.020	2.465±0.030	1.509±0.020	12300±200	7670±100	2.096±0.031	0.850±0.026	4.200±0.012	4.320±0.013	10.593±0.080
36	CF Tau	1.282±0.009	1.252±0.011	2.797±0.011	2.048±0.016	5200±150	6000±150	0.711±0.053	0.688±0.046	3.653±0.005	3.913±0.008	11.278±0.030
37	AG Per	4.498±0.134	4.098±0.109	3.009±0.070	2.616±0.070	18200±800	17400±800	2.950±0.087	2.751±0.092	4.134±0.025	4.215±0.027	13.815±0.091
38	SZ Cam	17.328±0.654	12.489±0.444	9.402±0.053	7.070±0.127	30360	27244±255	4.829	4.393±0.023	3.730±0.017	3.836±0.023	25.294±0.158
39	V818 Tau	1.047±0.165	0.758±0.108	0.898±0.189	0.767±0.099	5470	3977±22	-0.188	-0.879±0.130	4.552±0.259	4.548±0.152	16.176±0.050
40	BD-02 873	1.293±0.009	1.179±0.009	1.591±0.290	1.431±0.260	—	—	—	—	4.146±0.197	4.198±0.196	19.771±0.070
41	WW Cam	1.920±0.013	1.873±0.018	1.913±0.016	1.810±0.014	8360±140	8240±140	1.205±0.031	1.132±0.031	4.158±0.008	4.195±0.008	11.351±0.030
42	2MASS J04463285+1901432	0.467±0.050	0.192±0.020	0.560±0.020	0.210±0.010	3320±150	2900±150	-1.466±0.094	-2.553±0.112	4.611±0.060	5.077±0.066	2.659±0.080
43	2MASSJ04480963+0317480	0.567±0.002	0.532±0.002	0.552±0.008	0.532±0.006	3920±80	3810±80	-1.190±0.039	-1.271±0.040	4.708±0.013	4.712±0.010	3.828±0.010
44	TYC 4749-560-1	0.834±0.006	0.828±0.006	0.848±0.005	0.833±0.005	5340±200	5125±200	-0.280±0.071	-0.367±0.074	4.502±0.006	4.515±0.006	6.882±0.010
45	HP Aur	0.959±0.011	0.807±0.010	1.052±0.012	0.823±0.009	5790±80	5270±90	0.048±0.027	-0.329±0.032	4.376±0.011	4.514±0.011	6.435±0.020
46	V1236 Tau	0.788±0.010	0.771±0.008	0.766±0.015	0.803±0.010	4200±200	4133±250	-0.785±0.094	-0.772±0.121	4.566±0.018	4.516±0.012	9.200±0.100
47	CD Tau	1.441±0.016	1.366±0.016	1.798±0.017	1.584±0.020	6200±50	6200±50	0.632±0.017	0.522±0.018	4.087±0.010	4.174±0.012	13.517±0.070
48	AR Aur	2.474±0.098	2.288±0.093	1.781±0.036	1.816±0.036	10950±300	10350±300	1.612±0.054	1.531±0.057	4.330±0.025	4.279±0.025	18.240±0.230
49	EW Ori	1.173±0.011	1.123±0.009	1.169±0.005	1.098±0.005	6070±95	5900±95	0.222±0.028	0.118±0.029	4.372±0.006	4.407±0.005	20.194±0.050
50	2MASS J05282082+0338327	1.366±0.011	1.327±0.008	1.835±0.010	1.735±0.010	5103±26	4751±26	0.312±0.010	0.139±0.011	4.046±0.006	4.082±0.006	14.440±0.040
51	AS Cam	3.312±0.100	2.508±0.100	2.617±0.040	1.993±0.040	12000±600	10700±520	2.106±0.098	1.670±0.096	4.123±0.019	4.238±0.025	17.220±0.231
52	UX Men	1.235±0.006	1.196±0.007	1.349±0.013	1.275±0.013	6200±100	6150±100	0.383±0.030	0.320±0.031	4.270±0.009	4.305±0.009	14.686±0.030
53	TZ Men	2.482±0.025	1.500±0.010	2.017±0.020	1.433±0.015	10400±500	7200±300	1.631±0.093	0.695±0.080	4.224±0.010	4.302±0.010	27.933±0.080
54	V1174 Ori	1.01±0.0150	0.731±0.008	1.347±0.015	1.071±0.011	4470±120	3615±100	-0.187±0.050	-0.755±0.052	4.184±0.012	4.242±0.010	9.657±0.050
55	V432 Aur	1.080±0.016	1.224±0.016	2.464±0.020	1.232±0.006	6080±85	6685±8	0.872±0.026	0.435±0.005	3.688±0.010	4.345±0.007	11.770±0.030
56	GG Ori	2.342±0.016	2.337±0.017	1.852±0.025	1.830±0.025	9950±200	9950±200	1.480±0.038	1.469±0.039	4.272±0.012	4.282±0.012	24.846±0.060
57	V1031 Ori	2.281±0.017	2.467±0.018	4.349±0.034	3.006±0.064	7850±500	8400±500	1.809±0.128	1.606±0.120	3.519±0.008	3.874±0.019	16.012±0.040
58	beta Aur	2.369±0.027	2.295±0.027	2.762±0.017	2.568±0.017	9350±200	9200±200	1.719±0.039	1.628±0.040	3.930±0.007	3.980±0.008	17.600±0.060
59	V1388 Ori	7.421±0.080	5.156±0.030	5.604±0.040	3.763±0.030	20500±500	18500±500	3.697±0.045	3.173±0.050	3.812±0.008	3.999±0.007	16.491±0.050

Table 2. Continued.

ID	System	M_1 ($M/M_\odot$)	M_2 ($M/M_\odot$)	R_1 ($R/R_\odot$)	R_2 ($R/R_\odot$)	T_1 (K)	T_2 (K)	$\log L_1$ ($L/L_\odot$)	$\log L_2$ ($L/L_\odot$)	$\log g_1$ (cgs)	$\log g_2$ (cgs)	a ($R_\odot$)
60	FT Ori	2.168±0.022	1.773±0.020	1.871±0.013	1.626±0.013	9600±400	8600±300	1.426±0.079	1.113±0.066	4.230±0.008	4.265±0.009	14.286
61	V404 CMa	0.750±0.005	0.659±0.005	0.721±0.014	0.682±0.017	4200±100	3940±20	-0.838±0.047	-0.997±0.024	4.597±0.017	4.589±0.022	2.777±0.010
62	IM Mon	5.506±0.240	3.338±0.161	3.151±0.040	2.361±0.030	17500±350	14500±550	2.922±0.038	2.345±0.073	4.182±0.022	4.215±0.024	9.774±0.140
63	RR Lyn	1.935±0.008	1.520±0.004	2.579±0.020	1.596±0.030	7570±100	6980±100	1.292±0.025	0.735±0.031	3.902±0.007	4.214±0.017	29.424±0.040
64	V578 Mon	10.212±0.056	14.482±0.084	5.228±0.060	4.318±0.070	30000±500	26400±400	4.298±0.032	3.910±0.031	4.011±0.010	4.328±0.015	22.020±0.040
65	WW Aur	1.964±0.007	1.814±0.007	1.928±0.011	1.842±0.011	7960±420	7670±410	1.127±0.103	1.023±0.105	4.161±0.005	4.166±0.005	12.155±0.020
66	SV Cam	1.575±0.064	0.934±0.064	1.470±0.053	1.001±0.064	6038±58	4804±143	0.411±0.037	-0.320±0.083	4.301±0.038	4.408±0.068	4.037±0.032
67	GX Gem	1.488±0.011	1.467±0.010	2.334±0.012	2.244±0.012	6194±100	6166±100	0.857±0.029	0.815±0.030	3.875±0.006	3.903±0.006	15.314±0.030
68	HS Aur	0.898±0.019	0.877±0.017	1.005±0.023	0.874±0.030	5350±70	5200±72	-0.129±0.031	-0.300±0.040	4.387±0.022	4.498±0.032	23.360±0.150
69	HI Mon	11.426±0.241	9.864±0.162	4.775±0.102	4.645±0.065	30000±500	29000±500	4.220±0.036	4.137±0.034	4.138±0.021	4.098±0.014	15.786±0.102
70	LT CMa	5.591±0.200	3.364±0.140	3.600±0.070	2.046±0.050	17000±500	13140±800	2.988±0.057	2.049±0.124	4.073±0.024	4.343±0.029	12.737±0.201
71	SW CMa	2.240±0.014	2.105±0.018	3.015±0.020	2.496±0.042	8200±150	8100±150	1.567±0.034	1.382±0.037	3.830±0.006	3.967±0.015	32.071±0.080
72	HW CMa	1.719±0.011	1.779±0.012	1.649±0.018	1.668±0.021	7560±150	7700±150	0.902±0.037	0.944±0.037	4.239±0.010	4.244±0.011	48.810±0.100
73	GZ CMa	2.201±0.025	2.001±0.025	2.490±0.030	2.130±0.040	8810±350	8531±340	1.525±0.076	1.334±0.078	3.988±0.012	4.083±0.018	19.328±0.080
74	TYC 176-2950-1	1.058±0.008	1.043±0.008	1.653±0.030	1.182±0.020	—	—	—	—	4.026±0.016	4.311±0.015	27.547±0.100
75	CW CMa	2.093±0.020	1.977±0.020	1.906±0.040	1.805±0.071	—	—	—	—	4.199±0.019	4.221±0.036	11.081±0.010
76	FS Mon	1.632±0.012	1.462±0.010	2.061±0.012	1.637±0.012	6715±100	6550±100	0.890±0.027	0.646±0.028	4.023±0.006	4.175±0.007	9.426±0.010
77	YY Gem	0.598±0.005	0.601±0.005	0.621±0.006	0.605±0.006	3820±100	3820±100	-1.132±0.049	-1.155±0.049	4.629±0.009	4.653±0.009	3.898±0.010
78	2MASSJ07431157+0316220	0.584±0.002	0.544±0.002	0.559±0.002	0.512±0.004	3730±90	3610±90	-1.265±0.044	-1.398±0.046	4.710±0.003	4.755±0.007	5.864±0.020
79	PV Pup	1.539±0.012	1.527±0.014	1.536±0.016	1.493±0.016	6920±300	6930±300	0.686±0.083	0.664±0.083	4.253±0.010	4.274±0.010	8.574±0.040
80	V392 Car	1.900±0.024	1.853±0.024	1.624±0.030	1.600±0.031	8850±200	8650±200	1.162±0.045	1.109±0.046	4.296±0.017	4.298±0.018	14.129±0.050
81	CN Lyn	1.038±0.020	1.038±0.020	1.799±0.210	1.839±0.240	6500±250	6455±260	0.715±0.142	0.722±0.159	3.944±0.116	3.925±0.132	8.396±0.050
82	AI Hya	1.974±0.040	2.140±0.040	2.764±0.020	3.912±0.030	7100±60	6700±60	1.241±0.016	1.442±0.017	3.850±0.011	3.584±0.011	27.620±0.170
83	NSVS 07394765	0.360±0.005	0.180±0.004	0.459±0.004	0.491±0.005	3300±200	3106±125	-1.649±0.121	-1.696±0.077	4.671±0.010	4.311±0.013	5.912±0.505
84	TYC 5998-1918-1	0.703±0.003	0.687±0.003	0.694±0.009	0.699±0.013	4350±200	4090±200	-0.810±0.089	-0.911±0.096	4.602±0.012	4.586±0.017	6.232±0.010
85	AY Cam	1.947±0.041	1.707±0.036	2.784±0.020	2.034±0.015	7250±100	7395±100	1.284±0.025	1.046±0.025	3.838±0.011	4.054±0.011	12.677±0.090
86	VV Pyx	2.097±0.018	2.094±0.018	2.169±0.020	2.169±0.200	9500±200	9500±200	1.537±0.039	1.537±0.098	4.087±0.009	4.087±0.089	18.757±0.050
87	HD 71636	1.530±0.009	1.299±0.007	1.576±0.009	1.365±0.008	6950±140	6440±140	0.716±0.037	0.459±0.040	4.228±0.006	4.281±0.006	17.434±0.030
88	CU Cnc	0.427±0.002	0.394±0.001	0.433±0.005	0.392±0.009	3160±150	3125±150	-1.775±0.092	-1.881±0.096	4.796±0.010	4.847±0.020	7.775±0.010
89	VZ Hya	1.271±0.009	1.146±0.006	1.315±0.005	1.113±0.007	6645±150	6290±150	0.481±0.041	0.241±0.044	4.304±0.005	4.404±0.006	11.497±0.020

PASA, 31, e024 (2014)
doi:10.1017/pasa.2014.17

PASA, 31, e024 (2014)
doi:10.1017/pasa.2014.17

Table 2. Continued.

ID	System	M_1 ($M/M_\odot$)	M_2 ($M/M_\odot$)	R_1 ($R/R_\odot$)	R_2 ($R/R_\odot$)	T_1 (K)	T_2 (K)	$\log L_1$ ($L/L_\odot$)	$\log L_2$ ($L/L_\odot$)	$\log g_1$ (cgs)	$\log g_2$ (cgs)	a ($R_\odot$)
90	TZ Pyx	2.075±0.040	2.003±0.079	2.356±0.033	2.026±0.031	7468±203	7521±208	1.190±0.052	1.072±0.053	4.011±0.015	4.127±0.022	11.779±0.120
91	RS Cha	1.893±0.010	1.871±0.010	2.168±0.061	2.379±0.060	7638±76	7228±72	1.157±0.031	1.142±0.029	4.043±0.025	3.957±0.023	9.215±0.010
92	V467 Vel	30.699±1.023	9.459±1.051	12.09±1.008	5.037±1.007	37870	25500±500	5.431	3.984±0.227	3.760±0.081	4.010±0.233	28.310±0.201
93	NSVS 02502726	0.713±0.019	0.346±0.012	0.675±0.006	0.764±0.007	4300±200	3620±205	-0.854±0.090	-1.046±0.112	4.633±0.014	4.211±0.017	2.914±0.030
94	delta Vel	3.191±0.026	2.987±0.026	3.209±0.043	2.723±0.054	9450	9830	1.868	1.793	3.929±0.012	4.043±0.018	97.915±0.973
95	ASAS J085524-4411.3	1.204±0.003	1.056±0.002	1.871±0.020	1.635±0.016	—	—	—	—	3.975±0.009	4.035±0.009	20.288±0.220
96	CV Vel	6.076±0.074	5.977±0.070	4.130±0.024	3.912±0.027	18000±500	17780±500	3.206±0.051	3.138±0.052	3.990±0.007	4.030±0.008	34.937±0.150
97	XY UMa	1.097±0.073	0.665±0.031	1.161±0.020	0.630±0.010	5200±7	4125±7	-0.053±0.015	-0.986±0.014	4.349±0.034	4.662±0.025	3.112±0.060
98	PT Vel	2.199±0.016	1.626±0.009	2.095±0.020	1.560±0.020	9247±150	7638±180	1.460±0.030	0.871±0.045	4.138±0.009	4.263±0.012	9.746±0.020
99	KW Hya	1.973±0.036	1.485±0.017	2.129±0.015	1.486±0.022	8000±200	6900±200	1.222±0.046	0.653±0.055	4.077±0.010	4.266±0.014	24.924±0.120
100	2MASS J09381349-0104281	0.758±0.032	0.761±0.021	0.769±0.012	0.766±0.013	4360±150	4360±150	-0.717±0.066	-0.720±0.066	4.546±0.023	4.551±0.019	4.501±0.050
101	DU Leo	0.935±0.020	0.919±0.020	1.182±0.030	1.182±0.030	—	—	—	—	4.264±0.025	4.256±0.025	6.390±0.010
102	QX Car	9.246±0.120	8.460±0.120	4.293±0.060	4.053±0.060	23800±500	22600±500	3.725±0.040	3.585±0.043	4.139±0.014	4.150±0.014	29.801±0.210
103	HS Hya	1.255±0.008	1.219±0.007	1.278±0.007	1.220±0.007	6500±50	6400±50	0.418±0.014	0.351±0.015	4.324±0.006	4.351±0.006	7.682±0.010
104	ZZ UMa	1.179±0.013	0.960±0.010	1.518±0.023	1.158±0.013	5903±60	5097±60	0.400±0.023	-0.090±0.023	4.147±0.014	4.293±0.011	9.445±0.040
105	2MASS J10305521+0334265	0.499±0.002	0.444±0.002	0.457±0.005	0.427±0.004	3720±20	3630±20	-1.445±0.014	-1.546±0.013	4.816±0.010	4.825±0.008	5.733±0.020
106	UV Leo	1.126±0.090	1.080±0.097	0.958±0.024	1.197±0.042	6129±67	5741±59	0.065±0.030	0.145±0.037	4.527±0.043	4.315±0.053	3.898±0.089
107	RZ Cha	1.506±0.035	1.514±0.040	2.282±0.020	2.282±0.020	6457±160	6457±160	0.910±0.046	0.910±0.046	3.899±0.013	3.902±0.014	12.177±0.060
108	DW Car	11.341±0.120	10.626±0.140	4.561±0.045	4.299±0.055	27900±1000	26500±1000	4.054±0.068	3.913±0.072	4.175±0.010	4.198±0.013	14.238±0.050
109	UW LMi	1.156±0.022	1.136±0.022	1.269±0.052	1.248±0.062	6500±250	6500±250	0.412±0.083	0.397±0.088	4.294±0.038	4.301±0.046	13.687±0.062
110	GZ Leo	0.932±0.011	0.919±0.011	0.819±0.031	0.850±0.031	5120	5120	-0.383	-0.351	4.581±0.035	4.543±0.033	6.850±0.010
111	chi02 Hya	3.605±0.080	2.632±0.050	4.484±0.041	2.206±0.041	11750±190	11100±230	2.537±0.030	1.822±0.041	3.692±0.013	4.171±0.019	13.371±0.082
112	EM Car	22.833±0.319	21.376±0.329	9.356±0.170	8.345±0.160	34000±2000	34000±2000	5.021±0.118	4.922±0.118	3.855±0.017	3.925±0.018	33.742±0.150
113	LSPM J1112+7626	0.395±0.002	0.274±0.001	0.381±0.005	0.300±0.005	3061±162	2952±163	-1.942±0.104	-2.212±0.110	4.873±0.012	4.922±0.015	43.790±0.070
114	FM Leo	1.318±0.007	1.287±0.007	1.649±0.043	1.512±0.049	6316±240	6190±211	0.589±0.076	0.479±0.071	4.124±0.023	4.189±0.029	20.639±0.050
115	V346 Cen	11.744±1.393	8.344±0.795	8.252±0.302	4.227±0.201	26500±1000	24000±1000	4.479±0.080	3.726±0.093	3.675±0.065	4.107±0.063	39.117±1.801
116	MW UMa	1.257±0.095	1.124±0.091	1.258±0.010	1.138±0.010	6514±130	6112±22	0.408±0.037	0.210±0.010	4.338±0.035	4.377±0.038	6.468±0.010
117	EP Cru	5.019±0.130	4.830±0.130	3.590±0.035	3.495±0.034	15700±500	15400±500	2.847±0.060	2.790±0.061	4.029±0.014	4.035±0.015	44.828±0.370
118	IM Vir	0.981±0.012	0.664±0.005	1.062±0.016	0.681±0.013	5570±100	4250±130	-0.011±0.035	-0.867±0.060	4.378±0.014	4.594±0.017	5.944±0.020
119	HY Vir	1.838±0.009	1.404±0.006	2.830±0.008	1.532±0.008	7870	6546	1.441	0.588	3.799±0.003	4.215±0.005	12.174±0.555

Table 2. Continued.

ID	System	M_1 ($M/M_\odot$)	M_2 ($M/M_\odot$)	R_1 ($R/R_\odot$)	R_2 ($R/R_\odot$)	T_1 (K)	T_2 (K)	$\log L_1$ ($L/L_\odot$)	$\log L_2$ ($L/L_\odot$)	$\log g_1$ (cgs)	$\log g_2$ (cgs)	a ($R_\odot$)
120	eta Mus	3.283±0.040	3.282±0.040	2.140±0.020	2.130±0.040	12700±100	12550±300	2.029±0.016	2.005±0.047	4.294±0.010	4.297±0.017	14.111±0.150
121	NSVS 01031772	0.540±0.003	0.497±0.002	0.526±0.003	0.509±0.003	3615±72	3513±31	-1.372±0.036	-1.451±0.016	4.729±0.006	4.721±0.005	2.188±0.010
122	SZ Cen	2.272±0.025	2.311±0.021	4.555±0.023	3.622±0.021	8000±300	8280±300	1.883±0.071	1.743±0.068	3.478±0.007	3.684±0.006	17.931±0.060
123	ZZ Boo	1.616±0.010	1.568±0.010	2.164±0.070	2.164±0.070	6670±30	6670±30	0.920±0.030	0.920±0.030	3.976±0.029	3.963±0.029	18.083±0.050
124	BH Vir	1.178±0.018	1.050±0.015	1.228±0.050	1.118±0.040	6100±100	5500±200	0.273±0.048	0.012±0.077	4.331±0.038	4.362±0.033	4.803±0.020
125	DM Vir	1.454±0.008	1.448±0.008	1.764±0.017	1.764±0.017	6500±100	6500±300	0.698±0.029	0.698±0.089	4.108±0.009	4.106±0.009	16.771±0.030
126	V636 Cen	1.052±0.005	0.854±0.003	1.024±0.004	0.835±0.004	5900±85	5000±100	0.057±0.026	-0.408±0.036	4.440±0.004	4.526±0.004	13.764±0.020
127	Psi Cen	3.114±0.016	1.909±0.030	3.634±0.007	1.811±0.004	10450±300	8800±300	2.150±0.053	1.247±0.064	3.811±0.003	4.203±0.007	82.624±0.141
128	AD Boo	1.414±0.009	1.209±0.006	1.614±0.014	1.218±0.010	6575±120	6145±120	0.641±0.034	0.279±0.036	4.173±0.008	4.349±0.008	9.423±0.020
129	ASAS J150145-5242.2	1.767±0.021	1.771±0.021	2.875±0.141	2.825±0.141	—	—	—	—	3.768±0.045	3.784±0.046	21.120±0.111
130	GG Lup	4.106±0.040	2.504±0.024	2.379±0.025	1.725±0.019	14750±450	11000±600	2.381±0.057	1.592±0.108	4.299±0.010	4.363±0.011	11.901±0.060
131	GU Boo	0.609±0.007	0.599±0.006	0.628±0.016	0.625±0.020	3920±130	3810±130	-1.078±0.067	-1.131±0.071	4.627±0.023	4.624±0.029	2.781±0.010
132	CV Boo	1.045±0.013	0.995±0.012	1.269±0.023	1.180±0.023	5760±150	5670±150	0.202±0.051	0.111±0.052	4.250±0.017	4.292±0.018	4.778±0.020
133	alpha CrB	2.581±0.045	0.922±0.025	3.059±0.302	0.906±0.040	9700±200	5800±300	1.871±0.105	-0.079±0.111	3.879±0.096	4.489±0.042	42.852±0.322
134	RT CrB	1.344±0.010	1.359±0.009	4.256±0.074	3.778±0.064	5134±100	5781±100	1.053±0.039	1.156±0.035	3.309±0.016	3.417±0.015	17.409±0.029
135	ASAS J155259-6637.8	1.350±0.003	1.639±0.004	1.837±0.151	2.821±0.151	—	—	—	—	4.040±0.078	3.752±0.049	19.445±0.020
136	ASAS J155358-5553.4	1.847±0.006	1.927±0.006	2.731±0.280	2.991±0.300	—	—	—	—	3.832±0.100	3.771±0.097	20.887±0.010
137	V335 Ser	2.029±0.010	1.844±0.020	2.039±0.020	1.607±0.010	9506±289	8872±248	1.484±0.057	1.157±0.052	4.127±0.009	4.292±0.007	15.090±0.111
138	TV Nor	2.048±0.022	1.661±0.018	1.851±0.012	1.560±0.014	9120±148	7798±108	1.328±0.03	0.907±0.026	4.215±0.007	4.272±0.009	27.184±0.070
139	M4-V65	0.803±0.009	0.605±0.004	1.147±0.010	0.611±0.009	6088±108	4812±125	0.21±0.033	-0.745±0.050	4.224±0.009	4.648±0.013	8.203±0.020
140	M4-V66	0.784±0.004	0.743±0.004	0.934±0.005	0.830±0.005	6162±98	5938±105	0.053±0.029	-0.114±0.032	4.392±0.005	4.471±0.006	19.565±0.040
141	M4-V69	0.766±0.005	0.728±0.004	0.866±0.010	0.807±0.008	6084±121	5915±137	-0.035±0.038	-0.145±0.043	4.447±0.011	4.487±0.009	63.712±0.120
142	V760 Sco	4.969±0.090	4.610±0.070	3.028±0.060	2.656±0.050	16900±500	16300±500	2.827±0.058	2.650±0.060	4.172±0.019	4.253±0.018	12.886±0.091
143	ASAS J162637-5042.8	1.469±0.008	1.246±0.007	2.551±0.330	2.251±0.330	—	—	—	—	3.792±0.130	3.829±0.151	25.170±0.050
144	CM Dra	0.231±0.001	0.214±0.001	0.253±0.001	0.239±0.001	3130±70	3120±70	-2.258±0.041	-2.313±0.041	4.995±0.004	5.012±0.004	3.765±0.010
145	2MASS J16502074+4639013	0.490±0.003	0.486±0.003	0.907±0.120	0.905±0.100	3500	3395	-0.955	-1.010	4.213±0.134	4.211±0.109	4.504±0.020
146	V1292 Sco	26.257±0.424	10.385±0.142	12.581±1.236	5.841±3.033	31900±900	21800±4100	5.168±0.112	3.840	3.658±0.095	3.922	36.620±0.101
147	V1034 Sco	17.977±0.450	9.970±0.220	7.441±0.449	5.383±0.429	34000±150	26260±150	4.822±0.056	4.092±0.076	3.950±0.057	3.975±0.076	23.152±0.180
148	V2626 Oph	1.758±0.130	1.276±0.110	3.239±0.081	1.289±0.033	7760±64	7205±64	1.533±0.027	0.604±0.028	3.662±0.041	4.323±0.046	29.904±0.729
149	WZ Oph	1.227±0.007	1.220±0.006	1.401±0.012	1.419±0.012	6165±100	6115±100	0.406±0.03	0.403±0.030	4.234±0.008	4.221±0.008	14.724±0.020

PASA, 31, e024 (2014)
doi:10.1017/pasa.2014.17

Table 2. Continued.

ID	System	M_1 ($M/M_\odot$)	M_2 ($M/M_\odot$)	R_1 ($R/R_\odot$)	R_2 ($R/R_\odot$)	T_1 (K)	T_2 (K)	$\log L_1$ ($L/L_\odot$)	$\log L_2$ ($L/L_\odot$)	$\log g_1$ (cgs)	$\log g_2$ (cgs)	a ($R_\odot$)
150	V2365 Oph	1.964±0.017	1.055±0.010	2.191±0.009	0.934±0.004	9500±200	6400±210	1.545±0.038	0.119±0.061	4.050±0.005	4.521±0.006	17.465±0.050
151	V2368 Oph	2.417±0.018	2.525±0.065	3.857±0.019	3.740±0.019	9300±200	9500±200	2.000±0.039	2.010±0.038	3.649±0.005	3.695±0.012	81.493±0.653
152	U Oph	4.831±0.049	4.290±0.038	3.244±0.059	2.968±0.049	16900±1500	16000±1500	2.887±0.192	2.715±0.205	4.100±0.017	4.126±0.015	12.364±0.039
153	TX Her	1.607±0.040	1.441±0.030	1.688±0.030	1.428±0.030	7534±200	6678±211	0.916±0.052	0.561±0.062	4.189±0.019	4.287±0.021	9.878±0.060
154	LV Her	1.192±0.010	1.169±0.008	1.358±0.012	1.313±0.011	6060±150	6030±150	0.349±0.046	0.311±0.046	4.249±0.009	4.269±0.008	39.110±0.100
155	V624 Her	2.277±0.014	1.876±0.013	3.028±0.030	2.208±0.030	8150±150	7945±150	1.560±0.034	1.242±0.036	3.833±0.009	4.023±0.012	16.747±0.330
156	BD-00 3357	1.724±0.040	1.339±0.030	1.780±0.200	1.320±0.070	7250±30	6425±30	0.895±0.111	0.426±0.049	4.174±0.111	4.324±0.050	7.648±0.080
157	BD-11 4457	1.692±0.035	1.401±0.024	2.015±0.122	2.673±0.172	—	—	—	—	4.058±0.057	3.731±0.060	12.786±0.111
158	V539 Ara	6.265±0.070	5.326±0.060	4.436±0.120	3.735±0.250	18200±1300	16982±1215	3.287±0.149	3.018±0.165	3.941±0.025	4.020±0.063	20.549±0.070
159	V906 Sco	3.370±0.071	3.246±0.069	4.525±0.035	3.518±0.039	10400±500	10700±500	2.333±0.093	2.163±0.091	3.655±0.012	3.857±0.014	15.643±0.150
160	Z Her	1.611±0.070	1.312±0.030	1.859±0.060	2.743±0.080	6397±75	4977±175	0.716±0.036	0.618±0.072	4.107±0.035	3.680±0.028	15.142±0.171
161	V1647 Sgr	2.184±0.040	1.967±0.030	1.908±0.021	1.741±0.021	9600±310	9100±300	1.443±0.061	1.271±0.063	4.216±0.013	4.250±0.013	14.940±0.083
162	V3903 Sgr	27.204±0.549	18.964±0.439	8.120±0.086	6.149±0.060	38000±1900	34100±1700	5.091±0.098	4.662±0.097	4.054±0.013	4.138±0.013	21.876±0.211
163	EG Ser	2.200±0.050	1.990±0.030	1.689±0.010	1.549±0.010	9900±200	9100±200	1.391±0.037	1.169±0.040	4.325±0.011	4.357±0.009	31.383±0.200
164	V994 Her-B	1.868±0.120	1.859±0.120	1.583±0.080	1.493±0.080	9000±250	8450±70	1.169±0.071	1.009±0.052	4.311±0.055	4.359±0.058	8.243±0.149
165	V994 Her-A	2.828±0.200	2.299±0.160	2.123±0.049	1.688±0.039	12000±250	9450±90	1.924±0.043	1.310±0.027	4.236±0.038	4.345±0.038	11.837±0.247
166	V451 Oph	2.769±0.060	2.351±0.050	2.646±0.030	2.032±0.030	10800±800	9800±500	1.932±0.153	1.534±0.100	4.035±0.014	4.194±0.016	12.257±0.100
167	RX Her	2.748±0.090	2.326±0.064	2.458±0.111	1.998±0.111	11100	10016±71	1.916	1.557±0.053	4.096±0.044	4.204±0.053	10.616±0.111
168	UNSW-TR 2	0.512±0.034	0.529±0.036	0.646±0.050	0.613±0.060	—	—	—	—	4.527±0.080	4.587±0.101	7.033
169	V413 Ser	3.654±0.050	3.318±0.040	3.200±0.050	2.921±0.050	11100±300	10350±280	2.145±0.052	1.944±0.052	3.991±0.015	4.028±0.016	13.845±0.010
170	HD 172189	2.060±0.150	1.869±0.140	4.017±0.094	2.969±0.070	7920±15	7608±15	1.756±0.021	1.423±0.021	3.544±0.039	3.765±0.040	21.197±0.490
171	V1331 Aql	10.079±0.110	5.282±0.100	4.253±0.030	4.043±0.030	25400±100	20100±140	3.830±0.009	3.379±0.014	4.184±0.008	3.948±0.011	12.868±0.080
172	YY Sgr	3.897±0.130	3.482±0.090	2.576±0.030	2.344±0.050	14800±700	14125±670	2.456±0.092	2.293±0.094	4.207±0.018	4.240±0.022	15.605±0.201
173	BF Dra	1.413±0.003	1.374±0.003	2.999±0.017	2.763±0.017	6360±150	6400±150	1.121±0.043	1.061±0.043	3.634±0.005	3.693±0.005	29.669±0.014
174	BD+03 3821	4.261±0.116	2.819±0.114	3.830±0.030	2.073±0.020	13140±1500	12044±100	2.594±0.265	1.909±0.017	3.901±0.014	4.255±0.020	19.182±0.142
175	DI Her	5.173±0.100	4.524±0.060	2.679±0.050	2.479±0.050	16980±800	15135±715	2.729±0.093	2.462±0.093	4.296±0.019	4.305±0.019	43.170±0.240
176	HP Dra	1.056±0.005	1.024±0.007	1.340±0.012	1.028±0.010	6000±150	5895±150	0.320±0.047	0.059±0.048	4.208±0.008	4.424±0.009	26.185±0.039
177	BD-03 4412	1.814±0.006	1.513±0.005	1.701±0.300	1.501±0.400	—	—	—	—	4.235±0.189	4.265±0.331	20.270±0.010
178	V1182 Aql	30.884±0.598	16.592±0.400	9.059±0.181	4.892±0.181	43000±500	30500±500	5.401±0.027	4.269±0.045	4.014±0.020	4.279±0.035	21.037±0.302
179	V1665 Aql	3.965±0.399	3.656±0.370	4.131±0.100	2.601±0.060	12300±350	11650±310	2.545±0.057	2.049±0.054	3.804±0.051	4.171±0.051	20.456±0.450

PASA, 31, e024 (2014)
doi:10.1017/pasa.2014.17

Table 2. Continued.

ID	System	M_1 ($M/M_\odot$)	M_2 ($M/M_\odot$)	R_1 ($R/R_\odot$)	R_2 ($R/R_\odot$)	T_1 (K)	T_2 (K)	$\log L_1$ ($L/L_\odot$)	$\log L_2$ ($L/L_\odot$)	$\log g_1$ (cgs)	$\log g_2$ (cgs)	a ($R_\odot$)
180	V805 Aql	2.114±0.040	1.628±0.020	2.122±0.121	1.760±0.121	8185±330	7178±300	1.259±0.096	0.868±0.106	4.110±0.053	4.159±0.065	11.739±0.070
181	2MASS J19071662+4639532	0.679±0.010	0.523±0.006	0.634±0.043	0.525±0.052	4150	3700	-0.97	-1.334	4.666±0.064	4.716±0.096	18.535±0.080
182	V526 Sgr	2.275±0.070	1.683±0.060	1.901±0.020	1.569±0.020	10140±190	8710±100	1.535±0.035	1.105±0.023	4.237±0.016	4.273±0.019	10.282±0.181
183	KIC 4247791-1	1.700±0.020	1.538±0.010	2.508±0.010	2.408±0.010	—	—	—	—	3.870±0.006	3.862±0.005	15.952±0.040
184	KIC 4247791-2	1.301±0.020	1.261±0.020	1.464±0.130	1.354±0.120	—	—	—	—	4.221±0.085	4.276±0.085	14.631±0.040
185	FL Lyr	1.218±0.016	0.958±0.011	1.282±0.030	0.962±0.030	6150±100	5300±95	0.324±0.036	-0.183±0.043	4.308±0.022	4.453±0.028	9.164±0.040
186	TYC3121-1659-1	1.369±0.230	0.324±0.041	1.602±0.090	0.861±0.060	6700±150	3170±150	0.667±0.067	-1.173±0.116	4.165±0.098	4.079±0.091	5.617±0.060
187	V565 Lyr	0.995±0.003	0.929±0.003	1.101±0.007	0.971±0.009	5600±95	5430±125	0.030±0.031	-0.133±0.043	4.352±0.006	4.432±0.008	37.011±0.040
188	V568 Lyr	1.075±0.008	0.827±0.004	1.400±0.016	0.768±0.006	5665±100	4900±100	0.258±0.033	-0.515±0.038	4.177±0.011	4.585±0.007	30.962±0.060
189	V1430 Aql	0.957±0.010	0.859±0.020	1.101±0.010	0.851±0.010	5262±150	4930±100	-0.079±0.053	-0.416±0.038	4.335±0.009	4.512±0.015	4.693±0.020
190	UZ Dra	1.345±0.020	1.236±0.020	1.311±0.030	1.150±0.020	6210±110	5985±110	0.361±0.038	0.183±0.037	4.332±0.021	4.409±0.017	12.695±0.060
191	V2080 Cyg	1.190±0.017	1.156±0.017	1.596±0.008	1.599±0.008	6000±75	5987±75	0.472±0.023	0.470±0.023	4.108±0.008	4.093±0.008	16.205±0.070
192	V415 Aql	1.798±0.160	1.676±0.150	2.972±0.901	2.341±0.800	6590	6050	1.175	0.819	3.747±0.412	3.924±0.508	18.451±0.800
193	V2083 Cyg	2.159±0.139	2.105±0.114	2.293±0.184	2.650±0.216	7630	7623±45	1.204	1.328±0.078	4.052±0.082	3.915±0.082	10.350±0.162
194	WTS 19e-3-08413	0.463±0.025	0.351±0.019	0.480±0.022	0.375±0.020	3506±140	3338±140	-1.505±0.088	-1.805±0.096	4.741±0.049	4.835±0.055	5.539±0.120
195	V885 Cyg	2.000±0.029	2.228±0.026	2.487±0.013	3.591±0.028	8375±150	8150±150	1.436±0.033	1.708±0.034	3.948±0.008	3.676±0.009	9.674±0.032
196	WTS 19b-2-01387	0.498±0.019	0.481±0.017	0.496±0.013	0.479±0.013	3498±100	3436±100	-1.481±0.058	-1.542±0.060	4.744±0.029	4.760±0.029	5.472±0.080
197	WTS 19c-3-01405	0.410±0.023	0.376±0.024	0.398±0.019	0.393±0.019	3309±130	3305±130	-1.768±0.088	-1.781±0.089	4.851±0.051	4.825±0.053	11.266±0.270
198	KIC 6131659	0.922±0.007	0.685±0.005	0.880±0.003	0.640±0.006	5660±140	4780±105	-0.147±0.045	-0.717±0.041	4.514±0.004	4.661±0.009	33.261±0.060
199	V1143 Cyg	1.388±0.016	1.344±0.013	1.347±0.023	1.324±0.023	6460±100	6400±100	0.453±0.032	0.422±0.032	4.322±0.016	4.323±0.016	22.824±0.090
200	V541 Cyg	2.240±0.090	2.238±0.080	1.892±0.030	1.801±0.040	9885±230	9955±230	1.487±0.045	1.456±0.047	4.235±0.023	4.277±0.025	42.822±0.614
201	V1765 Cyg	24.873±0.348	12.191±0.240	21.189±0.780	5.897±0.217	—	—	—	—	3.182±0.034	3.983±0.034	79.059±0.420
202	V380 Cyg	13.015±0.586	7.488±0.269	15.344±0.209	3.904±0.073	21350±400	20500±500	4.643±0.036	3.383±0.048	3.181±0.023	4.129±0.023	61.794±0.835
203	BD-20 5728	1.646±0.008	1.187±0.006	2.741±0.130	2.031±0.110	—	—	—	—	3.779±0.043	3.897±0.050	21.881±0.040
204	KIC 10935310	0.678±0.021	0.347±0.012	0.614±0.007	0.898±0.012	4320±100	2750±65	-0.929±0.044	-1.383±0.045	4.693±0.017	4.072±0.019	10.918±0.020
205	BS Dra	1.360±0.083	1.358±0.098	1.442±0.022	1.423±0.072	6618±153	6626±153	0.554±0.044	0.545±0.064	4.254±0.031	4.265±0.058	13.187±0.255
206	V477 Cyg	1.772±0.119	1.329±0.069	1.580±0.050	1.278±0.040	8700±300	6700±235	1.109±0.071	0.471±0.072	4.289±0.042	4.349±0.037	10.839±0.272
207	V453 Cyg	14.377±0.200	11.119±0.130	8.564±0.055	5.497±0.063	26600±500	25500±800	4.518±0.034	4.060±0.059	3.730±0.008	4.004±0.011	30.636±0.170
208	2MASSJ20115132+0337194	0.557±0.001	0.535±0.001	0.519±0.011	0.456±0.007	3690±80	3610±80	-1.348±0.044	-1.499±0.043	4.754±0.019	4.849±0.014	3.186±0.009
209	TYC 4589-2999-1	1.815±0.101	0.838±0.105	2.011±0.040	0.846±0.020	5830±40	4616±116	0.623±0.022	-0.535±0.051	4.090±0.031	4.507±0.062	8.262±0.299

PASA, 31, e024 (2014)
doi:10.1017/pasa.2014.17

PASA, 31, e024 (2014)
doi:10.1017/pasa.2014.17

Table 2. Continued.

ID	System	M_1 ($M/M_\odot$)	M_2 ($M/M_\odot$)	R_1 ($R/R_\odot$)	R_2 ($R/R_\odot$)	T_1 (K)	T_2 (K)	$\log L_1$ ($L/L_\odot$)	$\log L_2$ ($L/L_\odot$)	$\log g_1$ (cgs)	$\log g_2$ (cgs)	a ($R_\odot$)
210	V478 Cyg	16.628±0.902	16.277±0.899	7.478±0.121	7.478±0.121	30550±1070	30550±1070	4.641±0.067	4.641±0.067	3.911±0.028	3.902±0.029	27.304±0.242
211	MY Cyg	1.805±0.030	1.794±0.030	2.215±0.020	2.275±0.020	7050±200	7000±200	1.037±0.053	1.048±0.053	4.004±0.011	3.978±0.011	16.266±0.080
212	V399 Vul	7.550±0.080	5.440±0.030	6.498±0.033	3.506±0.089	19000±320	18250±520	3.694±0.031	3.088±0.058	3.691±0.006	4.084±0.023	28.559±1.250
213	BP Vul	1.737±0.015	1.408±0.009	1.853±0.014	1.489±0.014	7709±150	6823±150	1.037±0.036	0.635±0.041	4.142±0.008	4.241±0.009	9.593±0.030
214	V442 Cyg	1.560±0.020	1.407±0.020	2.072±0.030	1.662±0.030	6900±82	6808±79	0.941±0.025	0.727±0.026	3.998±0.014	4.145±0.017	10.798±0.020
215	MP Del	1.559±0.085	1.248±0.074	2.429±0.046	1.576±0.030	7400±120	6927±120	1.201±0.034	0.710±0.036	3.860±0.030	4.139±0.032	45.668±0.820
216	V456 Cyg	1.863±0.060	1.580±0.050	1.681±0.020	1.471±0.020	7750±100	6755±400	0.962±0.025	0.607±0.118	4.257±0.018	4.302±0.019	5.885±0.060
217	MR Del	0.686±0.065	0.628±0.064	0.649±0.020	0.829±0.020	4900	4400±20	-0.662	-0.636±0.023	4.650±0.052	4.399±0.052	2.987±0.030
218	IO Aqr	1.624±0.020	1.520±0.020	2.538±0.060	2.089±0.130	6600	6425±300	1.040	0.825±0.110	3.840±0.022	3.980±0.058	10.953±0.040
219	V379 Cep	10.873±0.237	6.233±0.133	7.986±0.121	3.070±0.040	22025±428	20206±374	4.130±0.038	3.149±0.035	3.670±0.017	4.259±0.015	233.254±1.515
220	Y Cyg	17.275±0.395	17.275±0.300	6.006±0.300	5.706±0.300	31000±2000	31570±2000	4.476±0.141	4.463±0.139	4.118±0.047	4.163±0.049	28.489±0.120
221	CG Cyg	0.948±0.012	0.821±0.013	0.896±0.013	0.846±0.014	5260±185	4720±66	-0.258±0.067	-0.496±0.029	4.510±0.014	4.498±0.016	3.745±0.010
222	ER Vul	1.093±0.070	1.055±0.060	1.161±0.060	1.181±0.140	6000±52	5883±52	0.195±0.05	0.176±0.119	4.347±0.056	4.317±0.121	4.273±0.100
223	V1061 Cyg	1.281±0.015	0.931±0.007	1.616±0.017	0.974±0.020	6180±100	5300±150	0.534±0.031	-0.173±0.056	4.129±0.011	4.430±0.019	9.684±0.030
224	EI Cep	1.772±0.007	1.680±0.006	2.898±0.048	2.330±0.044	6750±100	6950±100	1.195±0.031	1.056±0.031	3.762±0.015	3.929±0.017	26.364±0.030
225	2MASS J21295384-5620038	0.839±0.017	0.714±0.013	0.847±0.012	0.720±0.017	4750±150	4220±180	-0.484±0.06	-0.831±0.085	4.506±0.015	4.577±0.023	3.851±0.020
226	BD-07 5586	1.096±0.030	1.036±0.030	1.269±0.230	1.239±0.220	—	—	—	—	4.271±0.196	4.267±0.191	17.227±0.240
227	EE Peg	2.151±0.020	1.332±0.010	2.103±0.030	1.321±0.010	8700±200	6450±300	1.357±0.044	0.433±0.090	4.125±0.013	4.321±0.007	12.150±0.060
228	EK Cep	2.024±0.020	1.122±0.010	1.579±0.015	1.315±0.015	9000±200	5700±190	1.167±0.041	0.215±0.063	4.348±0.009	4.250±0.011	16.628±0.080
229	OO Peg	1.759±0.031	1.700±0.030	2.204±0.081	1.379±0.050	8770±150	8683±180	1.412±0.046	0.987±0.051	3.997±0.034	4.389±0.034	13.195±0.070
230	VZ Cep	1.402±0.015	1.108±0.008	1.558±0.012	1.058±0.040	6670±160	5720±120	0.635±0.044	0.032±0.052	4.200±0.008	4.434±0.034	6.398±0.020
231	V497 Cep	6.473±0.432	5.000±0.371	3.713±0.030	2.938±0.030	19500±400	17756±405	3.253±0.038	2.887±0.043	4.110±0.031	4.201±0.035	10.736±0.382
232	BG Ind	1.502±0.008	1.343±0.008	2.326±0.017	1.706±0.039	6353±270	6653±233	0.898±0.081	0.709±0.069	3.882±0.007	4.102±0.021	7.688±0.010
233	CM Lac	1.971±0.060	1.503±0.100	1.509±0.030	1.549±0.030	9000±300	4586±160	1.128±0.065	-0.021±0.068	4.375±0.022	4.235±0.035	8.737±0.120
234	V398 Lac	3.834±0.350	3.291±0.320	4.893±0.180	2.452±0.110	11000±500	10900±450	2.498±0.095	1.882±0.090	3.643±0.054	4.176±0.062	24.946±0.781
235	BD-22 5866	0.594±0.029	0.594±0.029	0.616±0.045	0.600±0.045	—	—	—	—	4.633±0.073	4.656±0.075	7.567±0.512
236	BW Aqr	1.479±0.020	1.377±0.020	2.057±0.040	1.788±0.040	6350±100	6450±100	0.791±0.033	0.696±0.035	3.982±0.018	4.072±0.021	21.261±0.140
237	WX Cep	2.324±0.046	2.533±0.049	3.997±0.030	2.708±0.025	8150±225	8872±250	1.801±0.051	1.611±0.053	3.601±0.011	3.976±0.012	16.047±0.150
238	LL Aqr	1.223±0.058	1.055±0.051	1.325±0.020	1.005±0.016	6680±160	6200±160	0.497±0.046	0.127±0.050	4.281±0.025	4.457±0.026	41.040±0.620
239	RW Lac	0.928±0.006	0.870±0.004	1.193±0.004	0.970±0.004	5760±100	5560±150	0.148±0.031	-0.093±0.050	4.252±0.004	4.404±0.004	24.331±0.060

PASA, 31, e024 (2014)
doi:10.1017/pasa.2014.17

Table 2. Continued.

ID	System	M_1 ($M/M_\odot$)	M_2 ($M/M_\odot$)	R_1 ($R/R_\odot$)	R_2 ($R/R_\odot$)	T_1 (K)	T_2 (K)	$\log L_1$ ($L/L_\odot$)	$\log L_2$ ($L/L_\odot$)	$\log g_1$ (cgs)	$\log g_2$ (cgs)	a ($R_\odot$)
240	DH Cep	32.601±1.695	29.738±1.597	11.884±0.410	11.733±0.410	41000±2000	39550±2000	5.554±0.101	5.481±0.105	3.801±0.039	3.773±0.040	27.460±0.150
ID	System											
241	AH Cep	15.565±0.202	13.714±0.202	6.385±0.110	5.864±0.130	29900±1000	28600±1000	4.466±0.065	4.315±0.069	4.020±0.016	4.039±0.021	19.014±0.140
242	V364 Lac	2.334±0.015	2.296±0.025	3.308±0.038	2.986±0.035	8250±150	8500±150	1.658±0.034	1.621±0.034	3.767±0.010	3.849±0.011	26.519±0.080
243	V453 Cep	2.575±0.050	2.478±0.050	2.112±0.201	2.011±0.201	10300±500	10400±500	1.654±0.138	1.628±0.141	4.200±0.092	4.225±0.097	8.086±0.060
244	NY Cep	13.152±1.012	9.323±1.036	6.843±0.704	5.434±0.503	28500±1000	23100±1000	4.443±0.124	3.878±0.127	3.887±0.108	3.937±0.106	73.119±2.435
245	EF Aqr	1.244±0.008	0.946±0.006	1.338±0.012	0.956±0.012	6150±65	5185±110	0.362±0.020	-0.227±0.040	4.280±0.008	4.453±0.011	10.996±0.020
246	CW Cep	11.797±0.140	11.067±0.140	5.524±0.121	5.030±0.121	28300±1000	27700±1000	4.245±0.070	4.126±0.072	4.025±0.020	4.079±0.022	23.326±0.081
247	PV Cas	2.757±0.049	2.816±0.061	2.298±0.021	2.257±0.016	10200±250	10200±250	1.710±0.046	1.695±0.045	4.156±0.011	4.181±0.011	10.837±0.040
248	RT And	1.240±0.030	0.907±0.020	1.268±0.015	0.906±0.013	6095±214	4732±110	0.299±0.067	-0.432±0.044	4.325±0.015	4.481±0.016	3.986
249	V396 Cas	2.397±0.022	1.901±0.016	2.592±0.013	1.779±0.010	9225±150	8550±120	1.640±0.030	1.181±0.026	3.991±0.006	4.217±0.006	21.334±0.110
250	2MASS J23143816+0339493	0.469±0.002	0.383±0.001	0.441±0.002	0.374±0.002	3460±180	3320±180	-1.602±0.101	-1.817±0.106	4.820±0.004	4.876±0.005	5.733±0.020
251	NSVS 11868841	0.870±0.074	0.607±0.053	0.985±0.030	0.903±0.026	5250±135	5020±135	-0.179±0.055	-0.333±0.057	4.391±0.048	4.310±0.048	3.417±0.100
252	AR Cas	5.902±0.200	1.869±0.060	5.064±0.060	1.604±0.030	17200±500	8150±200	3.304±0.055	1.008±0.048	3.800±0.018	4.299±0.022	27.727±0.993
253	V731 Cep	2.577±0.098	2.017±0.084	1.823±0.030	1.717±0.025	10700±200	9265±220	1.592±0.037	1.290±0.045	4.328±0.022	4.273±0.023	23.276±0.290
254	IT Cas	1.330±0.009	1.328±0.008	1.603±0.015	1.569±0.040	6470±110	6470±110	0.607±0.032	0.588±0.039	4.152±0.009	4.170±0.023	14.436±0.040
255	BK Peg	1.414±0.007	1.257±0.005	1.985±0.008	1.472±0.017	6265±85	6320±30	0.736±0.025	0.492±0.013	3.993±0.004	4.202±0.010	18.173±0.200
256	AL Scl	3.617±0.110	1.703±0.040	3.241±0.050	1.401±0.020	13550±350	10300±360	2.502±0.050	1.297±0.067	3.975±0.019	4.376±0.016	13.335±0.150
257	V821 Cas	1.996±0.166	1.597±0.187	2.296±0.109	1.382±0.119	9400±400	8450±380	1.568±0.094	0.942±0.124	4.016±0.059	4.360±0.101	9.432±0.010

Table 3. Summary statistics of the present sample.

	Mass ($M/M_\odot$)	Radius ($R/R_\odot$)	$T_{\rm eff}$ (K)	log g (cms^{-2})	log L ($L/L_\odot$)	a ($R_\odot$)	q
Maximum	32.60	21.19	43000	5.077	5.554	233.25	1.114
Star (or system)	(1)	(2)	(3)	(4)	(1)	(5)	(6)
Minimum	0.18	0.21	2750	2.906	−2.553	1.85	0.237
Star (or system)	(7)	(8)	(9)	(10)	(8)	(11)	(12)
Mean	2.9	2.1	9500	4.20	2.8	18.9	0.851
Mode	1.3	1.3	6500	4.25	4.4	10.5	0.975
Median	1.5	1.7	6800	4.21	3.9	14.1	0.905
Errors							
Minimum	0.09%	0.19%	6	0.003	0.5%	0.01%	0.001
Maximum	16.8%	51.9%	4100	1.934	51%	8.54%	0.178
Mean	2.4%	3.2%	282	0.044	12.5%	0.44%	0.001
Mode	1.1%	0.9%	125	0.010	9%	0.02%	0.004
Median	1.3%	1.5%	150	0.016	10.1%	0.86%	0.007

(1) Primary of DH Cep; (2) primary of V1765 Cyg; (3) primary of V1182 Aql; (4) secondary of 2MASS J04463285+1901432; (5) V379 Cep; (6) V885 Cyg; (7) secondary of NSVS 07394765; (8) secondary of 2MASS J04463285+1901432; (9) secondary of KIC 10935310; (10) secondary of TZ For; (11) SDSS-MEB-1; (12) TYC3121-1659-1.

only one binary, EW Ori, has been re-studied later by Clausen et al. (2010). Thus, 92 binaries in both catalogues have common references from which catalogue parameters were taken. Therefore, catalogue values and accuracies must be similar. Nevertheless, we have noticed few small negligible differences most probably originating from the preferences among the multiple references. Additionally, few limited non-negligible differences exist because of identifying the primary and the secondary, which will be explained below while discussing the mass ratio (q) distribution of the present sample.

Statistics of masses, radii, effective temperatures, surface gravities, luminosity of individual stars, orbital semi-major axis (a), and mass ratio of binaries in the present sample are summarised in Table 3. Maximum and minimum values of those data with the identified star or the system are given in the first four rows. Following are mean, mode, and median values. Maximum, minimum, mean, mode, and median values of the associated errors are given in the last five lines. Relative errors are indicated by % sign after the value, otherwise the errors are absolute. Being related with characteristics of the present sample, some of the distributions will be discussed below.

2.3.1 Apparent magnitude and period distributions

Apparent magnitude distribution of the present sample (257 systems) is shown in Figure 1. Large range of apparent magnitudes, from very bright (1.89 mag, β Aur) to dimmest (19.92 mag, SDSS-MEB-1), display a peak at $V = 9$ mag, thus most of the systems are contained at 8, 9, or 10 mag.

The orbital period of the sample covers a range from $P_{\rm orb} = 0.30$ d (DV Psc) to $P_{\rm orb} = 99.7638$ d (V379 Cep). The distribution on the logarithmic scale is displayed in Figure 2. Accordingly, the most common orbital periods are close to 2.5 d. For a given mass, bigger orbital periods mean larger orbital sizes. Larger orbital size, however, decreases the probability of having eclipses. Since, our sample contains only eclipsing binaries, the decrease towards longer periods in Figure 2 is clear and it must be effected by the probability

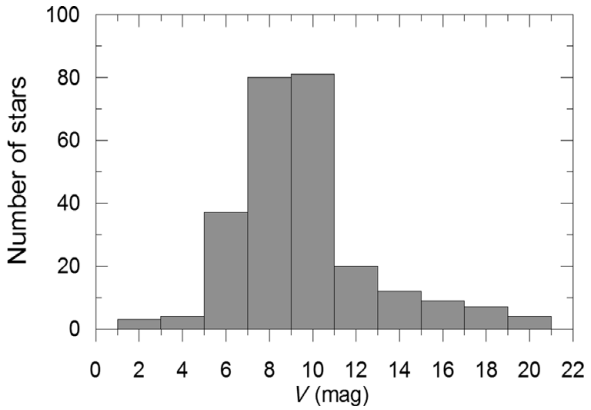

Figure 1. Apparent brightness distribution of 257 systems.

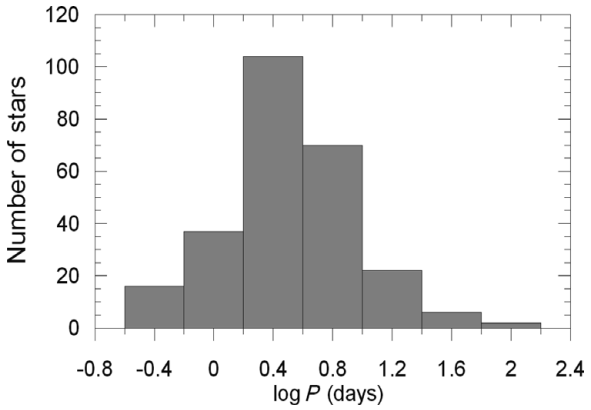

Figure 2. Orbital period distribution of 257 systems.

Table 4. Distribution of orbital periods among the spectral types of the primary components.

Spectral Type	O	B	A	F	G	K	M	Total
$-0.6 \leq \log P_{\rm orb} < -0.2$				1	3	5	5	14
$-0.2 \leq \log P_{\rm orb} < 0.2$		5	3	9	7	6	7	37
$0.2 \leq \log P_{\rm orb} < 0.6$	9	28	28	21	6	6	7	105
$0.6 \leq \log P_{\rm orb} < 1.0$	1	11	16	25	12	3	1	69
$1.0 \leq \log P_{\rm orb} < 1.4$		7	7	5	5			24
$1.4 \leq \log P_{\rm orb} < 1.8$			3	1	1		1	6
$1.8 \leq \log P_{\rm orb} < 2.2$		1		1				2
Total	10	52	57	63	34	20	21	257
Median $\log P_{\rm orb}$	0.44	0.43	0.53	0.60	0.67	0.18	0.18	
Median q	0.708	0.830	0.909	0.931	0.922	0.926	0.922	

of eclipses. Researchers prefer to study short-period systems because they are easier to observe. This is an additional bias to increase the number of systems towards the short periods. However, according to Figure 2, starting from $\log P_{\rm orb}$ (days) $= 0.4$, the number of systems decreases quickly towards the short periods. This could be explained by the fact that decreasing orbital period means decreasing the orbital sizes. Decreasing orbital size, however, increases the proximity effects such as, reflection and deviation from spherical shapes. Avoiding systems with proximity effects must be the main cause of the decrease towards short periods starting from the peak period $P_{\rm orb} = 2.5$ d.

Distribution of orbital periods among the spectral types (primary components) is given in Table 4. Shortest orbital periods (0.30 to 0.63 d) could be found among F and later spectral types. Such small orbital periods do not exist for the binaries with spectral types O, B, and A. The system with the smallest orbital period ($P_{\rm orb} = 0.30$ d, DV Psc) has components of spectral types K4V+M1V (Zhang & Zhang 2007).

Among the O-type binaries, the shortest orbital period is 1.62 d which belongs to V1182 Aql (Mayer, Drechsel, & Lorenz 2005), while the longest orbital period is only 4.24 d for V1292 Sco (Sana, Gosset, & Rauw 2006). It appears odd to find the maximum orbital period of O-type systems as short as 4.24 d. The long period cut-off for the B-type systems is at 99.76 d which is the orbital period of V379 Cep (Harmanec et al. 2007). Normally, larger radii would increase the probability of eclipses, thus, one would expect to see more O-type systems, and thus the median values of the orbital periods (Table 4) must increase towards earliest spectral types. However, the median $\log P_{\rm orb}$ decrease from G-type to O-type. Moreover, according to Table 4 (column 9), there are 247 binaries from B to M types. Consequently, 8 out of 247 with $\log P_{\rm orb}$ (days) > 1.4, and 32 out of 247 with $\log P_{\rm orb} > 1$; hence, probability to have chance 0 out of 10, which is the case for O-type systems, is 0.72 ($\log P_{\rm orb}$ (days) > 1.4) and 0.25 ($\log P_{\rm orb}$ (days) > 1), which is not compellingly low. These numbers might be biased somehow to very high values, but even computing only on the B-type stars (disadvantage of smaller subset), 1 out of 52 and 8 out of 52, gives probabilities of 0.82 ($\log P_{\rm orb}$ (days) > 1.4) and 0.19 ($\log P_{\rm orb}$ (days) > 1) to have no O-type stars at longer periods. The apparent lack of O-type stars at longer periods suffers from statistical significance because of the small size of this subset. However, inspecting the median values of mass ratios (Table 4), one may notice that the median value of mass ratio (q), is almost constant (median $q = 0.92$) for late spectral types (G, K, M), but it decreases from F-type to O-type as low as median $q = 0.708$. This implies that, O-type stars have higher probability to have a secondary with less massive than the primary. Combining this with faster rotation, the odds of detecting the secondary due to rotational broadening increases. Thus, faster rotation of O-type stars appears to be the main reason of finding them with the least number and smallest upper cut-off for the orbital periods on the Table 4.

2.3.2 Masses and radii

The distributions of masses and radii of 514 stars are shown in Figure 3. Similar appearance of both distributions is not a coincidence. This is because, almost all of the stars of the present sample are on the main sequence, only a few exceptions, e.g. BW Aqr, V379 Cep, RT CrB, TZ For, AI Hya, and V1292 Sco appear to have evolved components. Similar appearance implies a strong relation, which is commonly known as the main sequence mass-radius relation.

The uncertainty distributions of masses and radii are displayed in Figure 4. Figures 4a and 4c are in the accumulated form and Figures 4b and 4d are ordinary histograms showing the number of stars in 1% bin up to 20% uncertainty. Figures 4a and 4c indicate that in the sample there are 193 stars with masses better than 1% , 390 stars with masses better than 3% , and 443 stars with masses better than 5% uncertainties. Regarding the radii in the sample, there are 158 stars with radii better than 1% , 379 stars with radii better than 3% , and 437 stars with radii better than 5% uncertainties. The uncertainty range up to 20% includes all mass data, while the radii data contain 98% of sample stars in the same range. That is, there are only nine stars with uncertainties larger than 20% in radius.

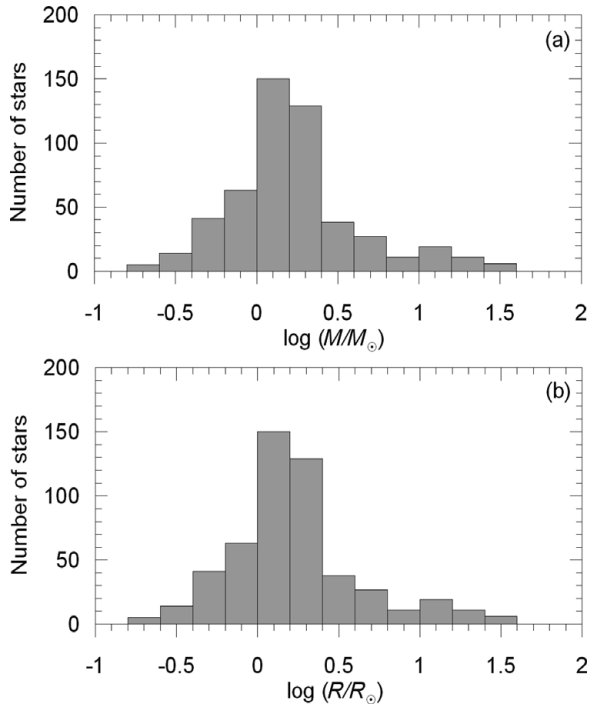

Figure 3. Distributions of masses (a) and radii (b) of 514 stars from 257 binaries.

2.3.3 Mass ratio and spectral types

The spectroscopic mass ratio (q) of the components is one of the most fundamental parameter of binary systems. It is conventionally defined as mass of the secondary divided by the mass of the primary. If the secondary is the less massive component, q is always less than one. Here, the light curve approaches are adopted; the primary is the eclipsed star during the primary minimum which is the deeper one of the two minima. Consequently, all mass ratios are determined spectroscopically from the radial velocity amplitudes as K_1/K_2.

The mass ratio distribution of the sample stars is displayed in Figure 5. The most common mass ratio of the sample is close to 0.9 and it is distributed within the range 0.2 to 1.2. The values $q < 1$ indicate more massive hotter primary and a cooler less massive secondary. This is the case for young unevolved binaries on the main sequence. On the other hand, the values $q > 1$ implies evolved pairs that more massive component cooler than the less massive secondary. Even when there would be no evolved pairs, some empirical mass ratios above unity are expected because of less precise systems with a q near unity. According to Figure 5, there are 21 systems with $q > 1$. Examining their positions on the H-R diagram, seven systems (TZ For, V1130 Tau, AI Hya, GZ Leo, RT CrB, V2368 Oph, V885 Cyg) were found for sure to have evolved cooler components. The rest have some ambiguity because one cannot identify the primary and the secondary due to component masses and/or temperatures so close.

Using published spectral types (Table S1) and counting each component as a single star, spectral-type distribution of 514 stars (257 pairs) is shown in Figure 6. Except for O-types, there exist statistically sufficient number of stars at all spectral types. The most crowded spectral types are F, A, and B. So, with an abrupt increase at B, number of stars increase until F, then there is a considerable sudden decrease to G, then gradual decrease towards M. Readers should be aware of that the papers announcing those spectral types (Table S1) use different kinds of estimates, from professional MK(K) types to very rough estimates, even from photometric indices.

The hottest star in the sample has an effective temperature of 43 000K which is the O-type primary of V1182 Aql (Mayer et al. 2005), while the coldest star in the sample has an

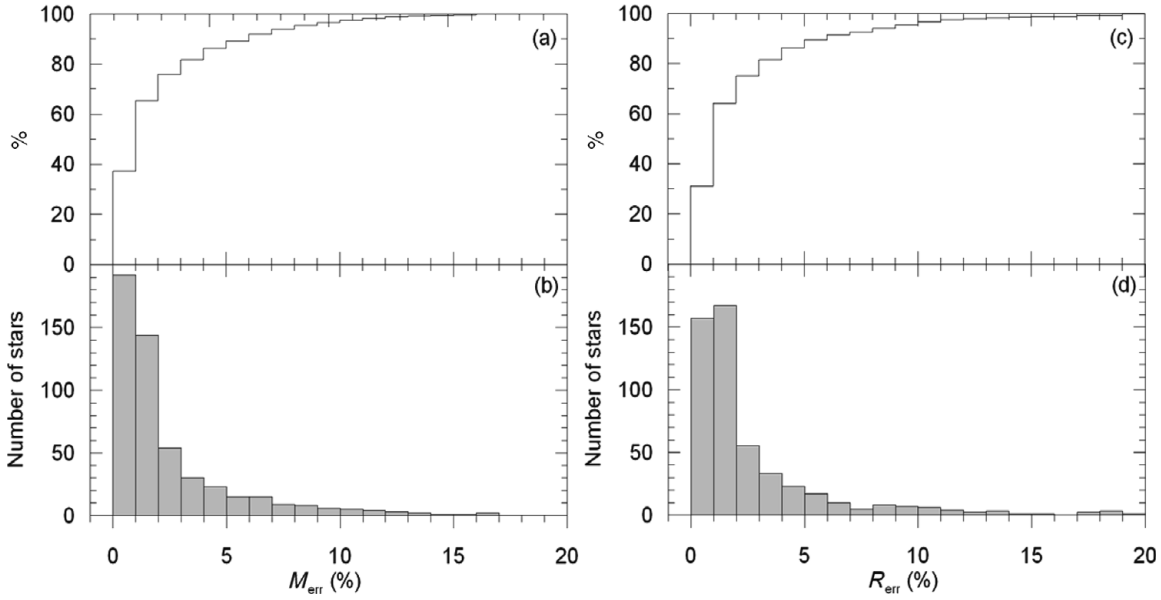

Figure 4. Uncertainty distributions of masses (a, b) and radii (c, d).

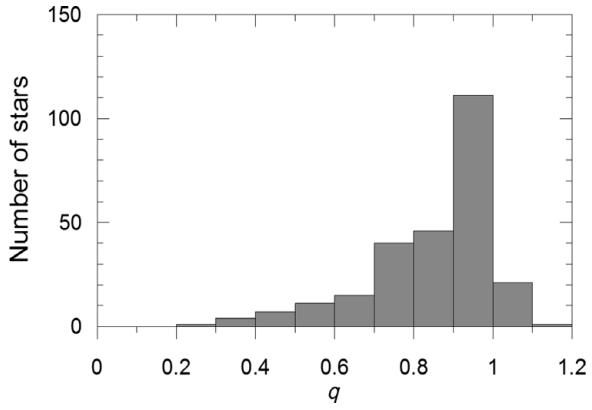

Figure 5. Mass ratio distribution of the sample. The median of q is 0.905.

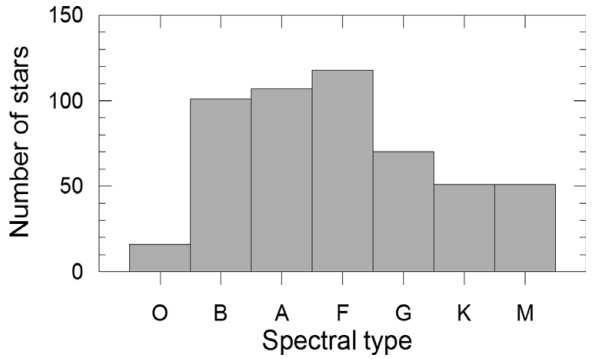

Figure 6. Distribution of 514 stars (257 pairs) according to spectral types.

effective temperature of 2 750 K which is M-type secondary of KIC10935310 (Çakırlı, İbanoğlu, & Sipahi 2013).

3 DISCUSSION

3.1 H-R diagram

The H-R diagram is a primary tool to demonstrate and study stellar evolution. Representing the stars with most accurate mass and radius, the present sample on the H-R diagram has been investigated. Taking the effective temperatures ($\log T_{\rm eff}$) from the catalogue (Table S1) and using the homogenised luminosities ($\log L_{\odot}$) from Table 2, the positions of 472 (236 binaries) stars on the H-R diagram are shown in Figure 7. Theoretical lines marking Zero Age Man Sequence (ZAMS) and Terminal Age Main Sequence (TAMS) from Pols et al. (1998) are drawn to indicate evolutionary status of the current sample. Almost the entire sample appears to be within the main-sequence band. Evidently, there are no supergiants despite the selection criteria not implying such a result directly. Considering the fact that evolved stars could be observed at larger distances than their main-sequence counterparts and the probability of having eclipses is higher if the radii of the components are larger, the absence of giants and supergiants in the present sample needs to be explained. Smaller number of evolved stars, which is a consequence of shorter lifetime of evolved phases, and low probability of evolving both components to the sizes comparable to each other, which permits the detection of eclipses, must be more effective than the eclipse favouring conditions. Obviously, much smaller size of companion stars exists, and/or huge difference of brightness between the components leave out some giants and supergiants to be detected as SB2 eclipsing binaries.

Although there are 514 stars (257 binaries) in the present sample, we are able to place 472 stars (236 binaries) with effective temperatures on the H-R diagram. This is because the catalogue (Table S1) has 21 systems (42 stars have no published temperatures; see Table S1) without temperatures. When solving the light and the radial velocity curves, some authors, who are not trusting stellar temperature determinations, are satisfied with the temperature ratios rather than absolute temperatures (i.e. Helminiak et al. 2009). The obtained masses and radii for those 21 systems are still reliable. Therefore, they were included in the catalogue.

Sample stars on H-R diagram were displayed as four subsamples according to accuracy limits. The four sub-samples [both mass and radius up to $\pm1\%$ accuracy (91 stars), between $\pm1\%$ and $\pm3\%$ (211 stars), between $\pm3\%$ and $\pm5\%$ (71 stars) and worse than $\pm5\%$ (99 stars)] were shown in Figure 7a with different symbols in order to investigate if there are any preferred positions among the data of different classes of accuracy. Except for the most accurate sub-sample (91 stars) which covers a spectral range from A0 to M3 corresponding to a temperature range 10 000 K to 3 000 K, the other sub-samples have full ranges covering spectral types from O5 to M3 and temperatures from 43 000 K to 3 000 K. Preference of certain locations by certain sub-samples cannot be noticed except for the most accurate sub-sample. All other sub-samples appear to be evenly distributed along the main-sequence band.

In order to investigate accuracy and precision of the positions on the H-R diagram (Figure 7), the published uncertainties of radii and temperatures have been propagated to estimate the uncertainty of the luminosities. Among the 472 stars (236 binaries) plotted on Figure 7a, the seven systems (2MASS J01542930+0053266, 2MASS J16502074+4639013, 2MASS J19071662+4639532, GZ Leo, HY Vir, δ Vel, V415 Aql) do not have published uncertainties for their temperatures and seven systems (V467 Vel, IQ Aqr, SZ Cam, RX Her, V2083 Cyg, MR Del, AE For) were found to have uncertainty of temperatures only for their secondaries. Leaving the systems without any temperature uncertainty out, and assigning same uncertainty to the primary temperature for those having only uncertainty for the secondary temperatures, the relative uncertainties of luminosities for 458 stars (229 binaries) were computed by the method of error propagation. All computed uncertainties are less than 51% except for one star, which is the secondary of V1292 Sco. The 18.8% uncertainty of the temperature and 51.9% uncertainty on the radius propagate to be 128% for the luminosity of this star. Among 458 stars, 87.6% (401 stars) have relative errors less than 20%. The rest, 57 stars

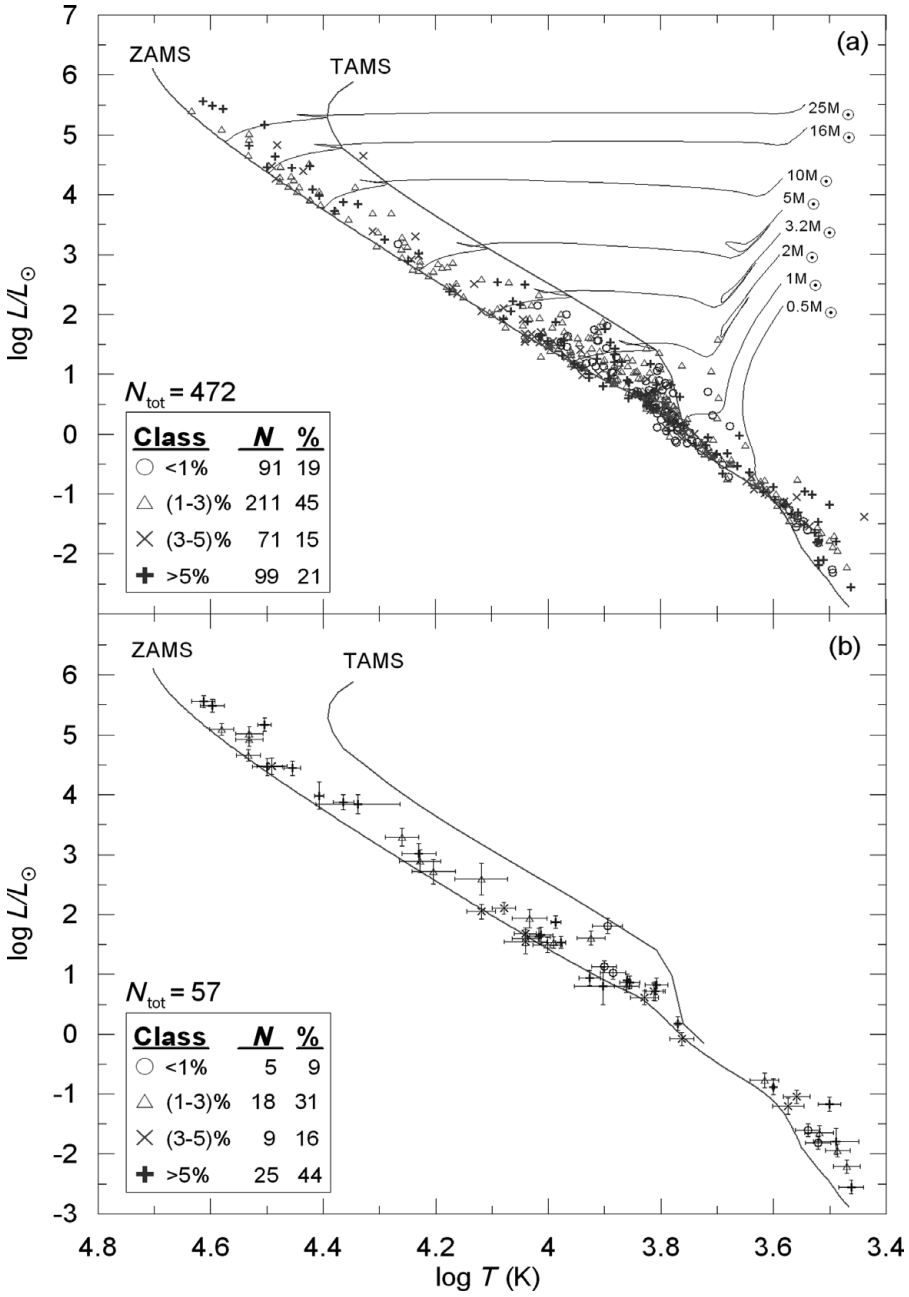

Figure 7. H-R diagram of 472 stars (a) and error bars (b) of 57 least accurate stars of the sample. Displayed error bars imply that most of the error bars in (a) are smaller than the symbols printed.

are placed on the H-R diagram with their error bars (Figure 7b) in order to investigate if certain locations are preferred by the stars with the biggest error bars. Even distribution along the main-sequence band covering the full range of spectral types is clear. However, one must remember that the most accurate sub-sample (91 stars) does not mean to have the most accurate positions on the H-R diagram because an uncertainty at an effective temperature contributes at both axes. Consequently there are contributions from all sub-samples to Figure 7b. Nevertheless, it is interesting to notice that the least accurate sub-sample dominates (44%) although it occupies only 21% (99 stars) among 472 stars in Figure 7a. The contributions to Figure 7b from the other three sub-samples are 5, 18, and 9, which sum up to be 56%, respectively from the groups of 91, 211, and 71 stars of the most accurate and the other two sub-samples in Figure 7a.

Determination of observed temperatures appears to be the biggest obstacle of observational astrophysics to study stellar evolution on the H-R diagram. Considering the fact that, some authors prefer to publish internal errors, which could be unrealistically small, e.g. the effective temperatures of AE For $T_{\rm eff}$(pri)= 4 100 ± 6 K and $T_{\rm eff}$(sec) = 4 055 ± 6 K

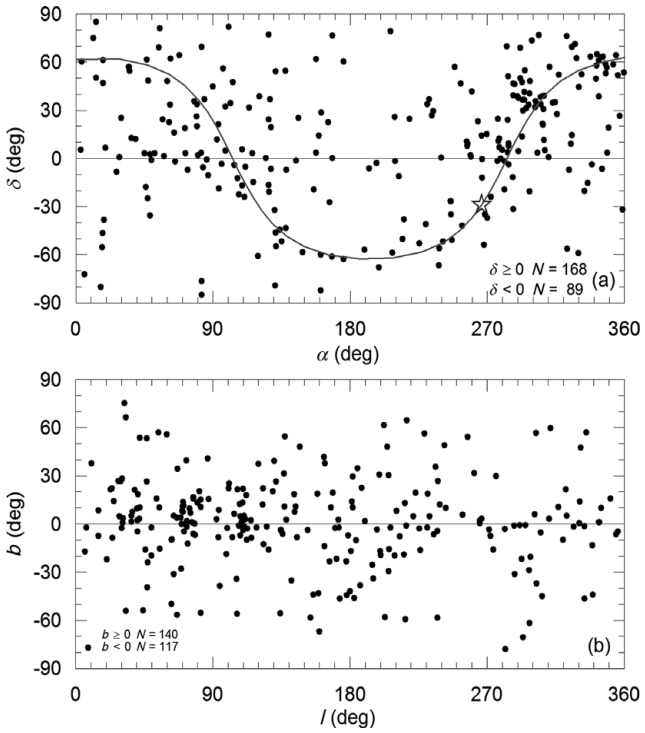

Figure 8. Distributions on the equatorial (a) and the Galactic (b) coordinates. Sinusoidal line in the upper panel is the Galactic plane, where the Galactic centre is marked as a big star symbol.

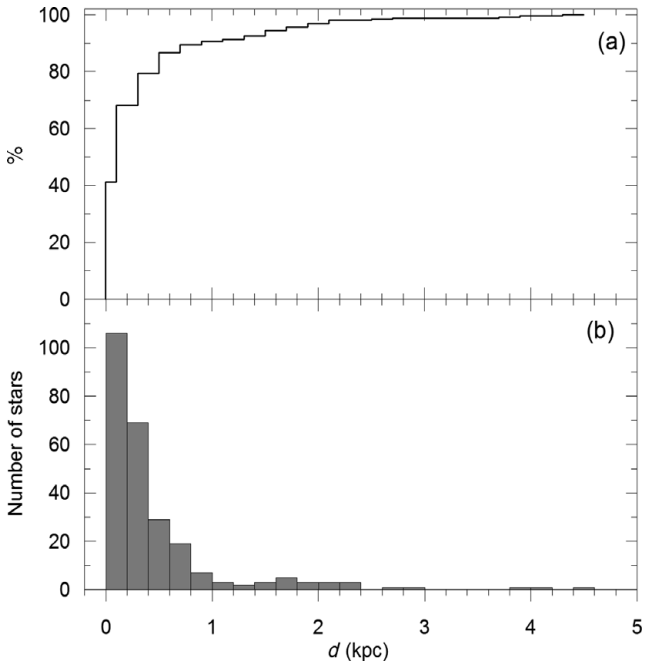

Figure 9. Distance distributions of the sample stars in the Solar neighborhood. (a) is in cumulative and (b) is in frequencies.

(Rozyczka et al. 2013), XY UMa $T_{\rm eff}$(pri) $= 5\,200 \pm 7$ K and $T_{\rm eff}$(sec) $= 4\,125 \pm 7$ K (Pribulla et al. 2001), and DV Psc $T_{\rm eff}$(pri) $= 4\,450 \pm 8$ K and $T_{\rm eff}$(sec) $= 3\,614 \pm 8$ K (Zhang & Zhang 2007), many of the uncertainties on the effective temperatures of the present sample are optimistic. But still, the present sample has the most accurate stellar positions on the H-R diagram ever obtained from the simultaneous solutions of light and radial velocity curves of detached eclipsing binaries and the stellar parameters would be the most reliable, thus, empirical relations and astrophysical theories could be tested.

3.2 Space distributions

Distributions of the present sample on the equatorial and the Galactic coordinates are displayed in Figure 8. Although 257 systems appear to be homogeneously distributed, a significant asymmetry between northern and southern hemispheres is indicated by the numbers in the lower right corner of Figure 8a. There exist 168 northern binaries with positive declinations ($\delta \geq 0^\circ$), while there are nearly half number of binaries in the southern hemisphere, that is, 89 systems with negative declination ($\delta < 0^\circ$). Detailed analysis is not in the scope of the present paper, but in the first approximation, the excess in the northern hemisphere could be explained by overpopulation of the northern telescopes and/or astronomers to the southern ones. Concentration of stars towards the Galactic plane is noticeable even on the equatorial coordinates that the Galactic plane drawn on Figure 8a, where the Galactic centre is marked by a star symbol.

Although a negligible north–south asymmetry is indicated by the numbers at the lower left corner, nearly symmetric distribution with respect to Galactic plane is shown in Figure 8b. It is also noticeable that there are regions on the Galactic plane where the stars appear to be grouping towards the Galactic longitudes 30, 70, and 110. These are the directions associated with the local arms structure of our Galaxy. On the other hand, less populated, 'empty region' towards $l = 250$, $b = -45^\circ$ are also noticeable in Figure 8b.

Among the 257 systems in the present sample, 205 systems were found to have distances published in articles from where catalogue data were taken. Therefore, we had to search extra sources for the distances of 52 systems, where 24 of them were found to have *Hipparcos* parallaxes (van Leeuwen 2007). For the rest with no trigonometric parallaxes, the formulae by Bilir et al. (2008a) were used in estimating distances. Finally, the distance distribution of the sample in the Solar neighborhood is presented in Figure 9. Figure 9b indicates the number of systems within each incremental 200 pc bins. Accumulated form of the same data (Figure 9a) indicates that 90% of sample stars are contained within 1 kpc from the Sun, where the rest are located at distances up to 4.6 kpc. Such distances are far more than the detection limit of *Hipparcos* (Perryman et al. 1997). In fact, excluding the parallaxes with large relative errors (e.g. $\sigma_\pi/\pi > 0.5$) in the sample, there are 119 systems (46.3%) with reliable parallaxes, thus, more than half (53.7%) of the sample had to rely on the photometric distances. Compared to other field stars,

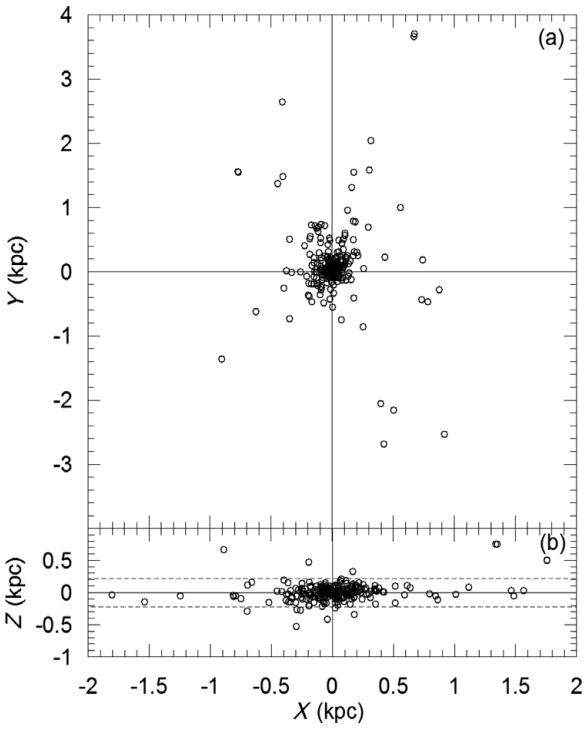

Figure 10. Distribution on the Galactic plane (a). X in the direction towards the Galactic centre, Y in the Galactic rotation. Distribution on the plane (X–Z) perpendicular to the Galactic disc (b). Dashed line represents the scaleheight of the thin disc. The scaleheight of the thin disc ($H = 220$ pc) is taken from Bilir et al. (2006a, 2006b).

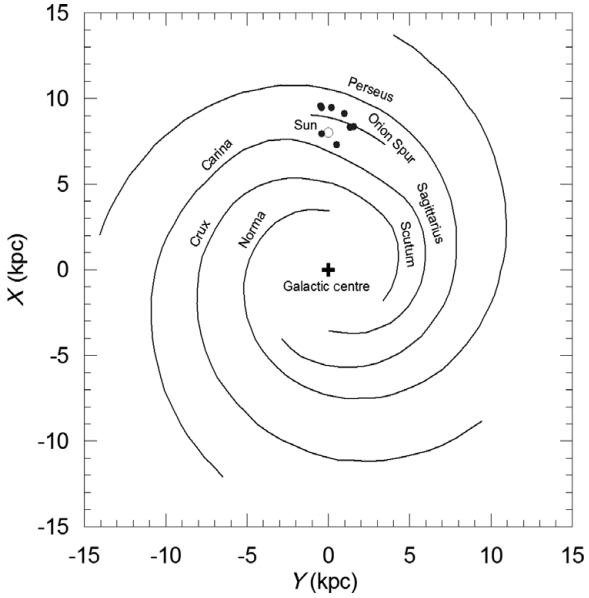

Figure 11. O-type binaries on the Galactic plane. The position of the spiral arms taken from Xu et al. (2009). It is assumed that the distance to the Galactic centre of the Sun is 8 kpc.

the present sample is advantageous to provide the most accurate photometric distances together with physical parameters.

Figure 10 displays space distribution of the sample in the Solar neighbourhood on the Galactic plane (X–Y), where X is towards the Galactic centre and Y is towards Galactic rotation. With a median distance of 1 528 pc, O-type binaries are the most distant objects. Closest one is SZ Cam which is 870 pc away (Tamajo et al. 2012), the most distant one is DH Cep with 2 767 pc (Hilditch, Harries, & Bell 1996). There exist 10 binaries with O-type primary in the present sample. The distant stars, mostly O-B type binaries on the X–Y plane were interesting (Figure 10a) as if to imply one of the local Galactic arms. Indeed, after plotting O-type binaries in our sample on Figure 11, which shows Galactic arm structure by Xu et al. (2009), the position of O-type binaries and the Sun on the Galactic plane became clear. The present sample is mostly located within 1 kpc in the Solar neighborhood which is itself positioned between the two local arms, Carina-Sagittarius and Orion Spur. The Orion spur itself is situated between the Perseus and Carina-Sagittarius arms.

Figure 10b shows the distribution perpendicular to the Galactic plane, where the scaleheight of the thin disc is $H =$ 220 pc according to Bilir et al. (2006a), Bilir, Karaali, & Gilmore (2006b), and Bilir et al. (2008b). Distant systems, mostly with O-B type binaries on the Galactic plane are distinguishable from the concentrated central region.

On a closer look, the space distribution of the concentrated region was shown in Figure 12. Unlike large-scale appearance, the very central region within 300 pc could be described evenly spread over the space. Nevertheless, even in this closer look the local Galactic disc structure is noticeable when the scaleheight lines were drawn in Figure 12b. One may easily notice that all local binaries ($d \leq 300$ pc) are contained within the thin-disc scaleheight limit except for only three systems.

3.3 How good single stars were represented?

The components of close binary systems with proximity effects are flattened at various degrees by fast rotation and tidally elongated towards each other by the mutual gravity in addition to irradiation effects. All these effects may be negligible in the case of detached binaries, where single star evolution could be applied to each component in better approximation. It is advantageous to know how good the present sample represents non-rotating spherical single stars of a given mass. However, the flattening due to rotation and the mass loss due to stellar winds may not be ignorable even for the case of single stars.

The tidal evolution forces the components of close binaries into tidal synchronisation. For interested readers, the catalogue contains projected rotational velocities ($v \sin i$), from which one can compute if tidal synchronisation was achieved. More importantly, rotation and Roche lobe filling ratio are two indicators for the component stars deviating from sphericity. For the sake of confidence, the sphericity of the present sample was inspected by computing the Roche model of each binary.

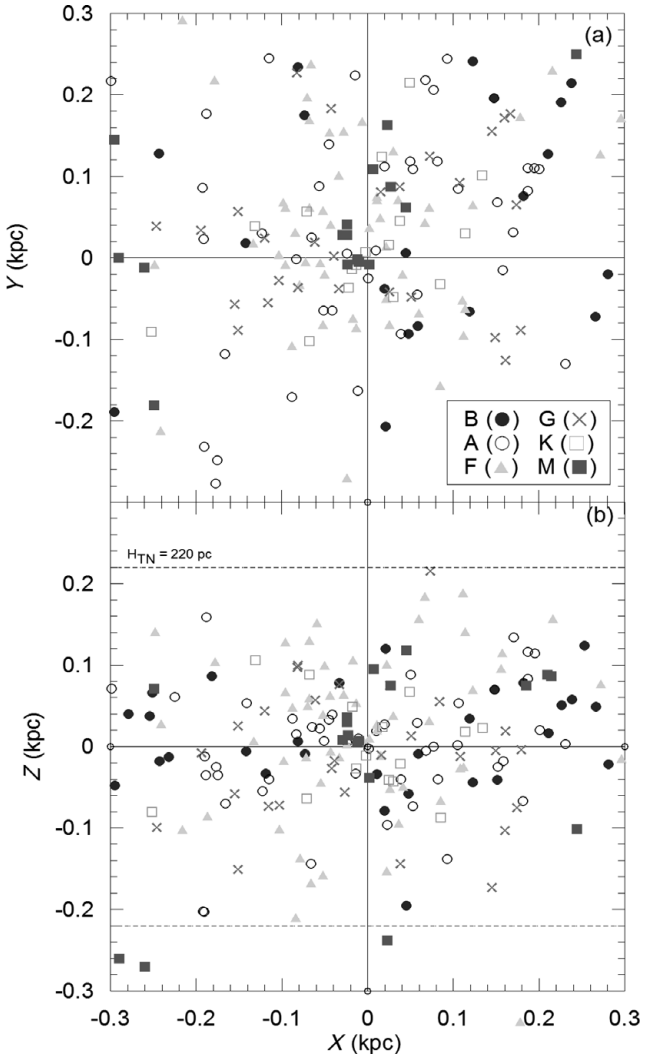

Figure 12. Nearby distributions of sample binaries within 300 pc.

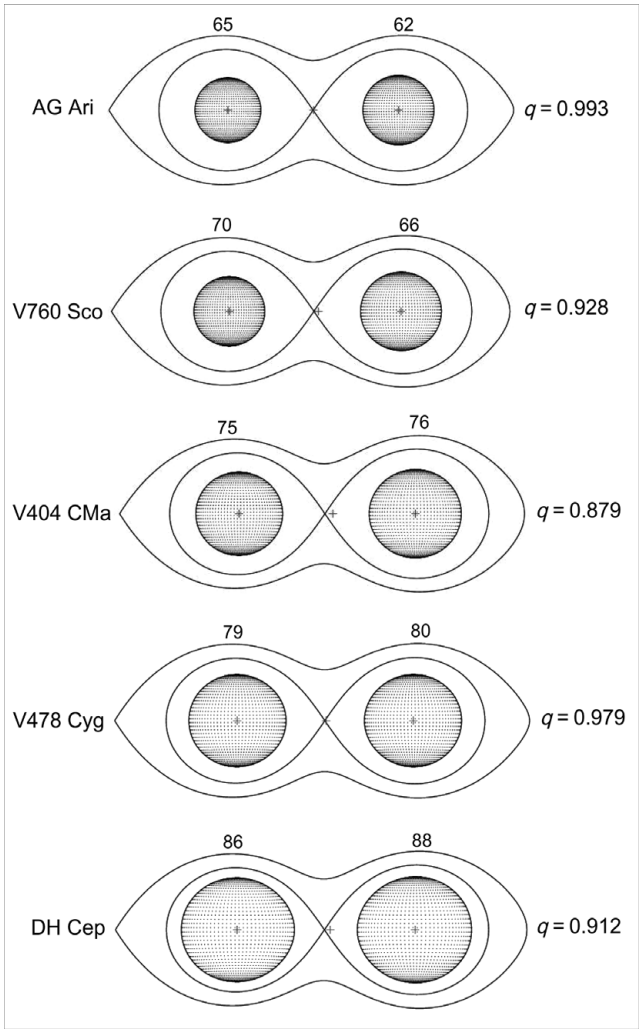

Figure 13. Examples of Roche lobe filling ratios. Names and mass ratios are at the sides, while filling ratio (FF, filling factor) is written on the top. By an eye inspection, one can notice sphericity spoils after FF 75.

Mass, mass ratio, and orbital period determine the sizes and the shapes of the Roche lobes (Kopal 1978). Classical definition of close (interacting) binary systems was given as $R_1 + R_2 \geq 0.1a$, where a is the semi-major axis of the orbit and $R_{1,2}$ are the radii of the components, the subscripts are for the primary and the secondary. The counter definition used for non-interacting binaries, $R_1 + R_2 < 0.1a$, however, implies the components are well-detached and very far from the proximity effects. Being well contained in the Roche lobes, their shapes are believed to be spherical. Unfortunately, the number of such systems is only 24 in the present sample and much less in previous samples (four in the list of Torres et al. 2010). In order to increase the number of detached systems, one prefers to loosen the condition $R_1 + R_2 < 0.1a$.

Equipotential surface of a component star is represented by four fractional radii defined as: r(side), r(back), r(point), and r(pole). The smallest of those is r(pole) and the largest one is r(point). The difference between those fractional radii increases by increasing filling ratio. In order to test and establish a well-structured limit for deviation from the sphericity we have computed Roche model of the sample binaries using Binary Maker[1]. This allowed us to compare fractional radii and make eye inspection of the shapes of the component.

Figure 13 displays how radii and shapes of the components change with respect to the Roche lobes from 60% filling to higher rates of filling factors (FF), which is defined as FF $= \bar{r}/\bar{r}_{RL}$, where $\bar{r}$ is average radius, and $\bar{r}_{\rm RL}$ is Roche-lobe radius relative to the semi-major axis. It can be deduced from an eye inspection that deviations from sphericity could be ignorable for small FF which can be up to 75% , a value corresponding to the difference between r(side) and r(pole) which is less than 1%. By the way, the difference between r(point) and r(side) being larger than 1% indicates tidal elongation and tidal synchronisation when $P_{\rm rot} = P_{\rm orb}$. By a careful look, eye could feel larger deviations (deviation $>$ 1% corresponding FF $>$ 75%), thus, non-spherical shapes of the component

[1] http://www.binarymaker.com/

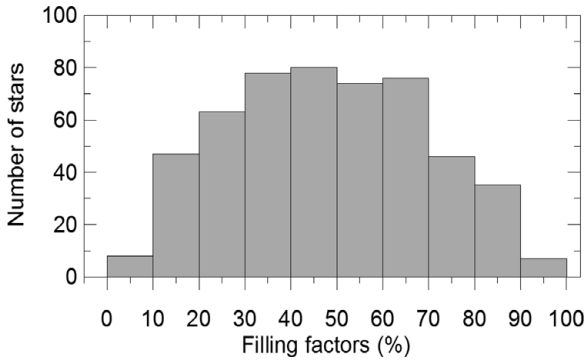

Figure 14. Distribution of the filling factors among 514 stars (257 binaries) of the sample.

stars of V478 Cyg and DH Cep in Figure 13 are noticeable. On the other hand, with less FF (FF < 75%), component stars of AG Ari and V760 Sco appear spherical.

The distribution of the filling ratios of the component stars in the present sample is displayed in Figure 14. Accordingly, 426 stars (82.9% of the sample) have FF less than 70% , which could be assumed to have spherical shapes. If one could expand sphericity limit to 75% FF , the number of spherical stars increases to 455 (88.5% of the sample). Overall, 20 binaries were found as both components exceed the limit of 75% FF , which includes seven O-type binaries. The number of binaries having at least one component above the limit 75% is 39, which includes nine O-type binaries. That is, 19 of these 39 binaries have only one component spherical, and the rest have both components non-spherical. We first attempted to discard the systems with non-spherical components. However, the number of O-type binaries was only 10 (3.9% of the sample). Among the 10, only one (Y Cyg, with $P_{\rm orb} = 2.996$ d) was found to have both components with spherical shapes. Therefore, we have decided not to discard the systems with more than 75% FF and left this choice to researchers, who may alter sphericity limit according to the their specific needs.

4 CONCLUSIONS

- The most accurate stellar parameters (masses, radii, temperatures, surface gravities, luminosities, projected rotational velocities, radial velocity amplitudes, mass ratio, orbital period, orbital inclination, semi-major axis, eccentricity) were compiled from the simultaneous solutions of light and radial velocity curves of detached double-lined eclipsing binaries.
- The masses and radii were homogenised using most recent values of $GM_{\odot} = 1.3271244 \times 10^{20}$ m^3 s^{-2} (Standish 1995) and $R_{\odot} = 6.9566 \times 10^8$ m (Haberreiter et al. 2008). Surface gravities and luminosities were recomputed using homogenised masses and radii.
- Apparent magnitudes, orbital periods, masses, radii, mass ratios, spectral types, and space distribution of the present sample were discussed.
- The number of stars with both mass and radius as accurate as 1% is 93, as accurate as 3% is 311, and as accurate as 5% is 388.
- Filling ratios of the current sample were studied. Thus, the geometrical shapes of the component stars were determined. Up to 75% of FF, stars are found almost spherical with 1% uncertainty.
- Giants and supergiants are missing in the present sample. Observational astronomers are encouraged to explore eclipsing binaries among giants and supergiants. Improving light curve observing techniques for discovering small amplitude SB2 eclipsing systems is a challenge

PASA, 31, e024 (2014)
doi:10.1017/pasa.2014.17

ACKNOWLEDGEMENTS

This work has been supported in part by the Scientific and Technological Research Council of Turkey (TÜBİTAK) grant numbers 106T688 and 111T224. Authors would like to thank anonymous referee who provided valuable comments for improving the manuscript and Mr. Muzaffer Karasulu for proof reading. This research has made use of the SIMBAD database, operated at CDS, Strasbourg, France and NASA's Astrophysics Data System. We would like to thank Dr. Nilda Oklay for helping online material.

REFERENCES

Andersen, J. 1991, A&ARv, 3, 91
Bilir, S., Karaali, S., Ak, S., Yaz, E., & Hamzaoğlu, E. 2006a, NewA, 12, 234
Bilir, S., Karaali, S., & Gilmore, G. 2006b, MNRAS, 366, 1295
Bilir, S., Cabrera-Lavers, A., Karaali, S., Ak, S., Yaz, E., & López-Corredoira, M. 2008b, PASA, 25, 69
Bilir, S., et al. 2008a, AN, 329, 835
Çakırlı, Ö., İbanoğlu, C., & Sipahi, E. 2013, MNRAS, 429, 85
Clausen, J. V., Bruntt, H., Olsen, E. H., Helt, B. E., & Claret, A. 2010, A&A, 511A, 22
Delfosse, X., Forveille, T., Ségransan, D., Beuzit, J.-L., Udry, S., Perrier, C., & Mayor, M. 2000, A&A, 364, 217
Demarque, P., Woo, J., Kim, Y., & Yi, S. K. 2004, ApJS, 155, 667
de Mink, S. E., Langer, N., & Izzard, R. G. 2011, Societe Royale des Sciences de Liege Bulletin, 80, 543
Duquennoy, A., & Mayor, M. 1991, A&A, 248, 485
Eddington, A. S. 1918, MNRAS, 79, 2
Eker, Z., et al. 2008, MNRAS, 389, 1722
Ekstrom, S., et al. 2012, A&A, 537A, 146
Girardi, L., et al. 2010, ApJ, 724, 1030
Gorda, S. Y., & Svechnikov, M. A. 1998, ARep, 42, 793
Haberreiter, M., Schmutz, W., & Kosovichev, A. G. 2008, ApJ, 675L, 53
Hall, D. S. 1994, International Amateur-Professional Photoelectric Photometry Communication, 54, 1
Harmanec, P. 1988, BAICz, 39, 329
Harmanec, P., et al. 2007, A&A, 463, 1061
Helminiak, K. G., Konacki, M., Ratajczak, M., & Muterspaugh, M. W. 2009, MNRAS, 400, 969
Hilditch, R. W., Harries, T. J., & Bell, S. A. 1996, A&A, 314, 165
Hillenbrand, L. A., & White, R. J. 2004, ApJ, 604, 741

Ibanoğlu, C., Soydugan, F., Soydugan, E., & Dervişoğlu, A. 2006, MNRAS, 373, 435
Kopal, Z. 1978, Dynamics of Close Binary Systems, Vol. 68 (Dordrecht: D. Reidel Publishing Co., Astrophysics and Space Science Library)
Kovaleva, D. A. 2001, ARep, 45, 972
Lastennet, E., & Valls-Gabaud, D. 2002, A&A, 396, 551
Malkov, O. Y. 1993, BICDS, 42, 27
Malkov, O. Y. 2003, A&A, 402, 1055
Malkov, O. Y. 2007, MNRAS, 382, 1073
Malkov, O. Y., Oblak, E., Snegireva, E. A., & Torra, J. 2006, A&A, 446, 785
Mayer, P., Drechsel, H., & Lorenz, R. 2005, ApJS, 161, 171
Perryman, M. A. C., et al. 1997, A&A, 323L, 49
Pols, O. R., Schröder, K.-P., Hurley, J. R., Tout, C. A., & Eggleton, P. P. 1998, MNRAS, 298, 525
Popper, D. M. 1980, ARA&A, 18, 115
Pribulla, T., Chochol, D., Heckert, P. A., Errico, L., Vittone, A. A., Parimucha, Š., & Teodorani, M. 2001, A&A, 371, 997
Ribas, I., Jordi, C., Torra, J., & Giménez, Á. 2000, MNRAS, 313, 99
Rozyczka, M., Pietrukowicz, P., Kaluzny, J., Pych, W., Angeloni, R., & Dékány, I. 2013, MNRAS, 429, 1840
Sana, H., Gosset, E., & Rauw, G. 2006, MNRAS, 371, 67
Shapley, H. 1914, ApJ, 40, 448
Standish, E. M. 1995, Highlights of Astronomy, 10, 180
Tamajo, E., Munari, U., Siviero, A., Tomasella, L., & Dallaporta, S. 2012, A&A, 539A, 139
Torres, G., Andersen, J., & Giménez, A. 2010, A&ARv, 18, 67
van Leeuwen, F. 2007, A&A, 474, 653
Xu, Y., Voronkov, M. A., Pandian, J. D., Li, J. J., Sobolev, A. M., Brunthaler, A., Ritter, B., & Menten, K. M. 2009, A&A, 507, 1117
Zhang, X. B., & Zhang, R. X. 2007, MNRAS, 382, 1133